


# Renal Effects of Dapagliflozin in People with and without Diabetes with Moderate or Severe Renal Dysfunction: Prospective Modeling of an Ongoing Clinical Trial<sup>§</sup>

 K. Melissa Hallow, David W. Boulton, Robert C. Penland, Gabriel Helmlinger, Emily H. Nieves, Daniël H. van Raalte, Hiddo L. Heerspink, and Peter J. Greasley

*Department of Chemical, Materials, and Biomedical Engineering, University of Georgia, Athens, Georgia (K.M.W., E.N.); Clinical Pharmacology and Quantitative Pharmacology, Clinical Pharmacology and Safety Sciences, R&D, AstraZeneca, Gaithersburg, Maryland (D.W.B.); Clinical Pharmacology and Quantitative Pharmacology, Clinical Pharmacology and Safety Sciences, R&D, AstraZeneca, Waltham, Massachusetts (R.C.P., G.H.); Diabetes Center, Department of Internal Medicine, Amsterdam University Medical Centers, location VUMC, Amsterdam, The Netherlands (D.H.v.R.); Department of Clinical Pharmacy and Pharmacology, University of Groningen, Groningen, Netherlands (H.L.H.); The George Institute for Global Health, Sydney, Australia (H.L.H.); and Early Clinical Development, Research and Early Development, Cardiovascular, Renal and Metabolism (CVRM) BioPharmaceuticals R&D, AstraZeneca, Gothenburg, Sweden (P.J.G.)*

Received March 27, 2020; accepted June 9, 2020

## ABSTRACT

Sodium glucose cotransporter 2 inhibitors (SGLT2i) reduce cardiovascular events and onset and progression of renal disease by mechanisms that remain incompletely understood but may include clearance of interstitial congestion and reduced glomerular hydrostatic pressure. The ongoing DAPASALT mechanistic clinical study will evaluate natriuretic, diuretic, plasma/extracellular volume, and blood pressure responses to dapagliflozin in people with type 2 diabetes with normal or impaired renal function (D-PRF and D-IRF, respectively) and in normoglycemic individuals with renal impairment (N-IRF). In this study, a mathematical model of renal physiology, pathophysiology, and pharmacology was used to prospectively predict changes in sodium excretion, blood and interstitial fluid volume (IFV), blood pressure, glomerular filtration rate, and albuminuria in DAPASALT. After validating the model with previous diabetic nephropathy trials, virtual patients were matched to DAPASALT inclusion/exclusion criteria, and the DAPASALT protocol was simulated. Predicted changes in glycosuria, blood pressure, glomerular filtration rate, and albuminuria were consistent with other recent studies in similar populations. Predicted albuminuria reductions were 46% in D-PRF, 34.8% in D-IRF, and 14.2% in N-IRF. The model predicts a similarly large IFV reduction

between D-PRF and D-IRF and less, but still substantial, IFV reduction in N-IRF, even though glycosuria is attenuated in groups with impaired renal function. When DAPASALT results become available, comparison with these simulations will provide a basis for evaluating how well we understand the cardiorenal mechanism(s) of SGLT2i. Meanwhile, these simulations link dapagliflozin's renal mechanisms to changes in IFV and renal biomarkers, suggesting that these benefits may extend to those with impaired renal function and individuals without diabetes.

## SIGNIFICANCE STATEMENT

Mechanisms of SGLT2 inhibitors' cardiorenal benefits remain incompletely understood. We used a mathematical model of renal physiology/pharmacology to prospectively predict responses to dapagliflozin in the ongoing DAPASALT study. Key predictions include similarly large interstitial fluid volume (IFV) reductions between subjects with normal and impaired renal function and less, but still substantial, IFV reduction in those without diabetes, even though glycosuria is attenuated in these groups. Comparing prospective simulations and study results will assess how well we understand the cardiorenal mechanism(s) of SGLT2 inhibitors.

## Introduction

Sodium glucose cotransporter 2 inhibitors (SGLT2i) have been shown to reduce cardiovascular (and particularly heart failure) events and improve renal outcomes in people with type 2 diabetes (T2D) (Zinman et al., 2015; Mosenzon et al., 2019). Although SGLT2 inhibition produces an initial hemodynamic drop in GFR, results from EMPA-REG, CANVAS, and DECLARE outcomes trials demonstrated that kidney

function in the treated groups stabilized, whereas the placebo group progressed (Wanner et al., 2016; Guthrie, 2018; Mosenzon et al., 2019). Post hoc analyses of phase III studies have found that dapagliflozin stabilized estimated GFR (eGFR) decline for up to 2 years (Fioretto et al., 2015) and reduced urinary albumin creatinine ratio (UACR) by 38%–48% in those with elevated albuminuria at baseline (Dekkers et al., 2018). Empagliflozin reduced the risk of new onset of macroalbuminuria, doubling of serum creatinine, and initiation of dialysis treatment, respectively (Wanner et al., 2016).

The mechanisms responsible for these cardiovascular and renoprotective effects remain incompletely understood.

This study was funded by AstraZeneca Pharmaceuticals.

<https://doi.org/10.1124/jpet.120.000040>

<sup>§</sup> This article has supplemental material available at [jpet.aspetjournals.org](http://jpet.aspetjournals.org).

Renoprotective mechanisms may include reduced glomerular hydrostatic pressure, reduced proximal tubule sodium transport both directly and through coupled NHE3 inhibition, and/or reduced blood pressure (Hallow et al., 2018a). In addition, sodium and glucose excretion with SGLT2i induces an osmotic diuresis, which could be responsible for improved heart failure outcomes (Hallow et al., 2018b).

Mathematical modeling provides a tool to describe, test, and quantitatively evaluate proposed mechanisms by which SGLT2 inhibition impacts renal and cardiovascular function. We have previously modeled the renal effects of dapagliflozin and identified a set of mechanisms capable of reproducing urinary and plasma biomarker responses observed in healthy subjects (Hallow et al., 2018a,b). Simulations with this model have demonstrated mathematically that SGLT2i reduces glomerular hydrostatic pressure as an indirect consequence of reduced proximal tubule sodium reabsorption (Vallon and Thomson, 2017). This provides a plausible explanation for the reduction in albuminuria and slowing of renal progression observed with SGLT2i. In addition, simulations predicted that SGLT2 inhibition will reduce interstitial fluid volume to a greater extent than blood volume compared with other forms of natriuretic/diuretic agents (Hallow et al., 2018a; Mahato et al., 2018). This suggests that in states of volume overload, such as heart failure, SGLT2 inhibition may relieve interstitial congestion without excessive lowering of blood volume and blood pressure, thus maintaining organ perfusion and possibly also preventing excessive neurohormonal activation.

Although SGLT2 inhibition has been shown to reduce total body fluid volume, no study has yet distinguished the relative effects of SGLT2 inhibition on blood and interstitial fluid volume during standardized sodium intake. The DAPASALT study (NCT03152084) is an open label, phase IV, three-arm mechanistic study designed to evaluate the natriuretic, diuretic, and blood pressure responses to 2 weeks of dapagliflozin treatment in people with T2D with and without renal impairment and in normoglycemic individuals with renal impairment. Data obtained from this study may allow clinical evaluation of model-based mechanistic hypotheses, including the relatively larger effect on interstitial fluid volume compared with blood volume. The true test of any mathematical model is its ability to prospectively predict behavior. In this analysis, we extend our existing model to prospectively simulate changes in urinary clinical chemistry variables, blood volume, interstitial fluid volume, GFR, and urinary albumin excretion rate (UAER) in the ongoing mechanistic clinical DAPASALT study. This will evaluate the extent to which we truly understand the renal mechanisms of SGLT2i and may also identify gaps in our existing knowledge.

## Methods

### Modeling Approach Overview

Using a previously developed mathematical model of renal function and diabetic kidney disease (Hallow et al., 2014, 2017, 2018a; Mahato et al., 2018), we generated a population of virtual patients with diabetes and varying degrees of kidney injury by varying model parameters associated with T2D, hypertension (a common comorbidity with diabetes), and kidney injury. Because the effects of T2D on kidney injury in the model were previously developed based on data from db/db mice with or without uninephrectomy (Mahato et al., 2018), we used human diabetic nephropathy clinical trial data to recalibrate rate constants for this component of the model and to validate the simulated response to standard-of-care therapies [i.e., ACE inhibitors (ACEI) and angiotensin receptor blockers (ARBs)]. We then selected a population of virtual patients to match the DAPASALT inclusion/exclusion criteria and simulated the protocol of the ongoing DAPASALT study.

### Model Description

The model of renal function and diabetic kidney injury is summarized in Fig. 1 and has been described in detail previously (Hallow and Gebremichael, 2017a,b; Hallow et al., 2018a; Mahato et al., 2018). This model describes the key physiologic processes of renal function and their roles in maintaining Na<sup>+</sup> and water homeostasis, as well as pathologic processes leading to renal injury and proteinuria in diabetes. Full model equations are also provided in the Supplemental Material. Here, we provide an overview of the model and describe only key model equations necessary to understand how renal injury and albuminuria were modeled, how parameters varied to generate virtual patients, and how SGLT2 inhibition was modeled.

**Renal Vasculature.** As shown in Fig. 1 (top left), the kidney is modeled as a set of nephrons in parallel.

Renal blood flow is a function of the mean arterial pressure (MAP), renal venous pressure, and renal vascular resistance, according to Ohm's law (Supplemental eqs. A1–A4). Renal vascular resistance is the equivalent resistance of preafferent, afferent, efferent, and peritubular arterioles and capillaries, and it also depends on the number of nephrons.

**Glomerular Filtration.** Single nephron glomerular filtration rate (SNGFR) depends on the glomerular ultrafiltration coefficient ( $K_f$ ) as well as the net filtration pressure across the glomerulus, according to Starling's equation:

$$SNGFR = K_f (P_{gc} - P_{Bow} - \pi_{go-avg}) \quad (1)$$

Here,  $K_f$  is the glomerular ultrafiltration coefficient,  $P_{gc}$  is glomerular capillary hydrostatic pressure,  $P_{Bow}$  is pressure in the Bowman's space, and  $\pi_{go-avg}$  is average glomerular capillary oncotic pressure. The total GFR is then the SNGFR multiplied by the number of nephrons ( $N_{nephrons}$ ):

$$GFR = SNGFR * N_{nephrons} \quad (2)$$

**ABBREVIATIONS:** ACE, angiotensin converting enzyme; ACEI, ACE inhibitor; Ang, angiotensin; ARB, angiotensin receptor blocker; AT1, Angiotensin Type 1; AT2, Angiotensin Type 2; CANAVAS, CANagliflozin cardioVascular Assessment Study; AVOID, Aliskiren in the Evaluation of Proteinuria in Diabetes;  $C_{glu}$ , plasma glucose concentration; CKD, chronic kidney disease; D-IRF, patients with type 2 diabetes with impaired renal function; D-PRF, patients with type 2 diabetes with preserved renal function; eGFR, estimated GFR; EMPAREG, Empagliflozin Cardiovascular Outcome Event Trial in Type 2 Diabetes Mellitus Patients; GFR, glomerular filtration rate; IDNT, Irbesartan Diabetic Nephropathy Trial; IFV, interstitial fluid volume; MAP, mean arterial pressure; NESTOR, Natrilix SR versus Enalapril Study in Type 2 diabetic hypertensives with microalbuminuria; NHE3, sodium-hydrogen exchanger 3; N-IRF, normoglycemic with impaired renal function;  $\mu_{other,seiv}$ , podocyte injury;  $\Delta Perm$ , change in glomerular membrane permeability;  $P_{gc}$ , glomerular capillary hydrostatic pressure; PT, proximal tubule; RAAS, renin-angiotensin-aldosterone system; RENAAL, Reduction of Endpoints in NIDDM with the Angiotensin II Antagonist Losartan Study;  $RC_{albumin}$ , proximal tubule capacity to reabsorb a filtered albumin; SGLT, sodium glucose cotransporter; SGLT2i, SGLT2 inhibitor; SNGFR, single nephron glomerular filtration rate; T2D, type 2 diabetes; UACR, urinary albumin creatinine ratio; UAER, urinary albumin excretion rate; UGE, urinary glucose excretion.

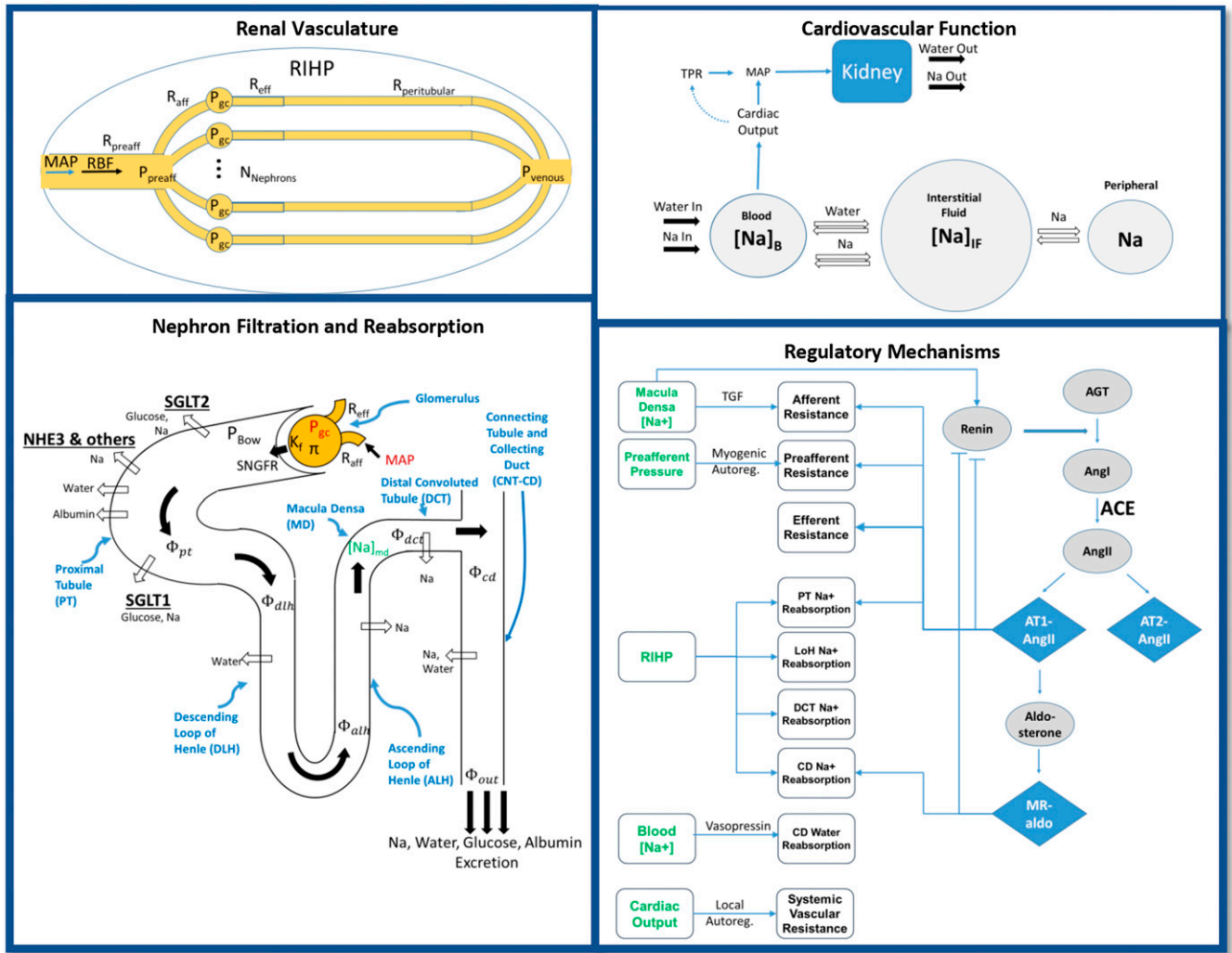


**Fig. 1.** Base model of renal function. (Top left) The renal vasculature is modeled by a single preafferent resistance vessel flowing into  $N$  parallel nephrons. (Bottom left) Glomerular filtration is modeled according to Starling's law.  $\text{Na}^+$  and water are reabsorbed at different fractional rates in the proximal tubule, loop of Henle, distal convoluted tubule, and connecting tubule/collecting duct. Glucose and  $\text{Na}^+$  reabsorption are coupled through SGLT2 and SGLT1 in the proximal tubule. (Top right) The balance between  $\text{Na}^+$  and water excretion and intake determine blood volume and  $\text{Na}^+$  concentration.  $\text{Na}^+$  and water move between the blood and interstitial fluid across a concentration gradient, and  $\text{Na}^+$  may be sequestered nonosmotically in a peripheral storage compartment. Blood volume determines venous return and cardiac output, which together with total peripheral resistance, determine mean arterial pressure and subsequently renal perfusion pressure, closing the loop. (Bottom right) Multiple regulatory mechanisms, including the RAAS and tubuloglomerular feedback (TGF), provide feedback on model variables to maintain or return homeostasis.  $\Phi$ , flow rate; CD, collecting duct; CNT-CD, connecting tubule and collecting duct; DLH, descending loop of Henle;  $N_{\text{Nephron}}$ , number of nephrons;  $P_{\text{Bow}}$ , pressure in the Bowman's space;  $R_{\text{aff}}$ , afferent arteriole resistance; RBF, renal blood flow; RIHP, renal interstitial hydrostatic pressure set point;  $R_{\text{preaff}}$ , preafferent arteriole resistance;  $P_{\text{venous}}$ , venous pressure; LoH, loop of Henle;  $R_{\text{peritubular}}$ , peritubular capillary resistance; TPR, total peripheral resistance. Adapted from Hallow et al. (2017).

**Glucose Filtration, Reabsorption, and Excretion.** Glucose is filtered freely through the glomerulus. Thus, the filtered load for a single nephron is the product of SNGFR and average plasma glucose concentration ( $C_{\text{glu}}$ ):

$$\Phi_{\text{glu,filtered}} = \text{SNGFR} \cdot C_{\text{glu}}. \quad (3)$$

Glucose is reabsorbed by SGLT2 in the S1 and S2 segments of the proximal tubule (PT) and by SGLT1 in the S3 segment, up to the reabsorptive capacity of each segment (Supplemental eqs. A8 and A9). Any unreabsorbed glucose then flows through the rest of the tubule and is excreted in the urine (Supplemental eq. A10).

**$\text{Na}^+$  Filtration and Reabsorption.** The single nephron-filtered  $\text{Na}^+$  load is given by:

$$\Phi_{\text{Na,filtered}} = \text{SNGFR} \cdot C_{\text{Na}} \quad (4)$$

where  $C_{\text{Na}}$  is the plasma  $\text{Na}^+$  concentration.  $\text{Na}^+$  is reabsorbed through different transporters at different rates in each segment

along the tubule. In the proximal tubule, NHE3 plays a major role in  $\text{Na}^+$  reabsorption, and thus NHE3 reabsorption is modeled explicitly. In addition, coupling of glucose and  $\text{Na}^+$  reabsorption through SGLT2 and SGLT1 at a 1:1 molar ratio (Supplemental eq. A12) and by SGLT1 at a 1:2 molar ratio (Supplemental eq. A13) is modeled. Additional  $\text{Na}^+$  reabsorption through other transporters is also accounted for (Supplemental eqs. A14–A18). For the remaining nephron segments, we approximate  $\text{Na}^+$  reabsorption in each segment as distributed uniformly along the length and defined by a fractional rate of reabsorption (Supplemental eqs. A15–A18).

Dapagliflozin treatment is not associated with changes in serum potassium, so for simplicity, potassium filtration and reabsorption were not tracked in the model (Yavin et al., 2016).

**Water Reabsorption.** Water reabsorption in the PT is isosmotic. Thus, the rate of water reabsorption depends on the concentration of osmolytes, including  $\text{Na}^+$  and glucose, in the tubular fluid (Supplemental eqs. A19–A21).

The flow rates of osmolytes and water out of the PT are then used to determine water reabsorption along the remaining nephron segments, including regulation by vasopressin in the collecting duct, as described previously and in the Supplemental eqs. A22–A28.

**Blood and Interstitial Fluid and Peripheral Sodium Storage.** Sodium and water are modeled as distributed between the blood, interstitium, and a third compartment that stores  $\text{Na}^+$  nonosmotically (Fig. 1 (top right)) (Titze, 2009, 2014; Hammon et al., 2015; Hallow et al., 2018b). Sodium and water are assumed to move freely between the blood and interstitial fluid across a  $\text{Na}^+$  concentration gradient. Water and sodium intake rates are assumed constant. Then, blood volume and blood sodium are the balance between intake and excretion of water and sodium, respectively, and the intercompartmental transfer between blood and interstitium (Supplemental eqs. A29 and A30). Similarly, interstitial fluid volume (IFV) depends on the intercompartmental transfer between blood and interstitium (Supplemental eq. A31).

When interstitial sodium concentration exceeds the normal equilibrium level,  $\text{Na}^+$  is assumed to move out of the interstitium and is sequestered in the peripheral  $\text{Na}^+$  compartment, where it is osmotically inactive. Thus, the change in interstitial fluid sodium depends on intercompartmental transfer and peripheral storage (Supplemental eqs. A32–A34). Sodium cannot be stored indefinitely; thus, there is a limit on how much sodium can be stored.

**Albumin Filtration, Reabsorption, and Excretion.** The rate of albumin filtration is a function of SNGFR, the plasma albumin concentration  $C_{\text{albumin}}$ , and the sieving coefficient  $K_{\text{albumin}}$ , as described in Lazzara and Deen (2007):

$$\Phi_{\text{albumin,filtered}} = K_{\text{albumin}} * \text{SNGFR} * C_{\text{albumin}} \quad (5)$$

The PT has limited capacity to reabsorb a filtered albumin ( $RC_{\text{albumin}}$ ), beyond which excess albumin is excreted.

$$\Phi_{\text{albumin,reabs}} = \min(\Phi_{\text{albumin,filtered}}, RC_{\text{albumin}}). \quad (6)$$

The UAER is then

$$\text{UAER} = (\Phi_{\text{albumin,filtered}} - \Phi_{\text{albumin,reabs}}) * N_{\text{nephrons}}. \quad (7)$$

**Kidney Injury.** Nephron loss due to kidney injury was modeled by reducing the number of nephrons. Although nephron loss in kidney disease is progressive, we did not account for progressive nephron loss in the current analysis, since all simulation durations were less than 6 months.

We assumed that, when glomerular capillary hydrostatic pressure  $P_{gc}$  rises above some normal limit  $P_{gc,0}$ , it causes injury and dysfunction of the glomerulus and podocytes. The magnitude of this injury signal ( $GP_{\text{injury}}$ ) is defined as:

$$GP_{\text{injury}} = \max(P_{gc} - P_{gc,0}, 0). \quad (8)$$

Glomerular hypertension causes glomerular hypertrophy, with up to a 50% increase in glomerular volume observed within a few weeks in diabetic and/or nephrectomized rats, mice, and humans (Flyvbjerg et al., 2002; Levine et al., 2008; Bivona et al., 2011). The ultrafiltration coefficient  $K_f$  in eq. 1 above reflects both the permeability and surface area of the glomerular membrane. The effect of glomerular hypertension on  $K_f$  through changes in the glomerular surface area (hypertrophy) is modeled as

$$\frac{d}{dt}(\Delta SA) = (\Delta SA_{\text{max}} - \Delta SA) * \frac{GP_{\text{injury}}}{\tau_{SA}}. \quad (9)$$

$\Delta SA_{\text{max}}$  is the maximum increase in glomerular surface area (SA; expressed as a percentage), and  $\tau_{SA}$  represents the time constant for the increase in surface area.  $\Delta SA_{\text{max}}$  is fixed at 50%, and the time constant  $\tau_{SA}$  is set so that a steady state is reached within a few weeks.

Glomerular hypertension also contributes to progressive glomerulosclerosis, which is a slower process than glomerular hypertrophy. Mathematically, this can be represented as a decrease in glomerular permeability  $\Delta \text{Perm}$ , so that the ultrafiltration coefficient  $K_f$  is given by

$$K_f = K_{f,0} * (1 + \Delta SA - \Delta \text{Perm}) \quad (10)$$

where  $K_{f,0}$  is the normal ultrafiltration coefficient in the healthy state. For this analysis, we assume that progression of glomerulosclerosis over the simulation period (6 months or less) is minimal. Thus,  $\Delta \text{Perm}$  is treated as a parameter representing damage that has already accrued but does not change during the simulation.

Glomerular hypertension also damages podocytes, causing them to leak protein. Reversible glomerular hypertensive injury to podocytes is modeled as a sigmoidal function:

$$\mu_{\text{gp,seiv}} = \frac{E_{\text{max}} GP_{\text{injury}}^\gamma}{GP_{\text{injury}}^\gamma - K_{m,\text{gp,seiv}}^\gamma}. \quad (11)$$

There may some podocyte injury that is irreversible or that is due to nonhemodynamic mechanisms. This is represented by a parameter  $\mu_{\text{other,seiv}}$ . The albumin sieving coefficient is then given by

$$K_{\text{albumin}} = K_{\text{albumin},0} * (1 + \mu_{\text{gp,seiv}} + \mu_{\text{other,seiv}}) \quad (12)$$

where  $K_{\text{albumin},0}$  is the sieving coefficient under normal conditions. Changes in albumin excretion are assumed to reflect near-instantaneous (within hours to days) changes in glomerular hypertension. This is consistent with the fast changes in proteinuria observed with antihypertensive treatments and in diseases such as preeclampsia (Mikami et al., 2014).

**Regulatory Mechanisms.** The model incorporates key intrinsic and neurohormonal regulatory feedback mechanisms, as illustrated in Fig. 1 (bottom right). 1) Tubuloglomerular feedback is modeled as a signal from macula densa sodium flow (Supplemental eq. A45) that signals the afferent arteriole (Supplemental eq. A1) to constrict or relax. 2) Myogenic autoregulation is modeled as a function of preafferent pressure (Supplemental eqs. A46 and A47) that signals the preafferent arterioles (Supplemental eq. A1) to constrict or relax. 3) Vasopressin is modeled as a function of plasma  $\text{Na}^+$  concentration (Supplemental eq. A48) that alters collecting duct water reabsorption (Supplemental eq. A25). 4) The pressure natriuresis phenomenon is modeled as a signal from renal interstitial hydrostatic pressure (Supplemental eqs. A49 and A50) that alters  $\text{Na}^+$  reabsorption rates along the nephron (Supplemental eqs. A14 and A16). 5) Whole-body blood flow autoregulation is modeled as a signal from cardiac output that modulates peripheral resistance (eq. 12; Supplemental eq. A51). 6) To describe the renin-angiotensin-aldosterone system (RAAS), renin secretion is modeled as a function of macula densa sodium flow, with a strong inhibitory feedback from angiotensin II (AngII) bound to the Angiotensin Type 1 (AT1) receptor (AT1-bound AngII) (Supplemental eqs. A52–A55). Renin generates angiotensin I, which can be converted to AngII by ACE or chymase, or degraded (Supplemental eq. A56). AngII can bind to the AT1 or Angiotensin Type 2 (AT2) receptor, or it can be degraded (Supplemental eq. A57). AT1-bound AngII signals efferent, preafferent, and afferent vasoconstriction; PT sodium retention; and aldosterone secretion (Supplemental eq. A59). Aldosterone binds to the mineralocorticoid receptor (Supplemental eq. A60) and signals sodium retention in the connecting tubule/collecting duct (Supplemental eq. A61).

**SGLT2 Inhibition.** As described previously, the direct effect of 10 mg dapagliflozin once daily on SGLT2 was modeled as a constant 85.3% inhibitory effect on the glucose reabsorption rate per unit length through SGLT2 in the S1 and S2 segments (Supplemental eq. S68, used above in Supplemental eq. S8) (Hallow et al., 2018a). After initiating treatment with SGLT2i, urinary glucose excretion (UGE) reaches a maximum within 24 hours and then settles to a stable level slightly less than peak over the next several days. This is assumed to

be in part due to compensation as SGLT1 and 2 are upregulated, and as described previously (Hallow et al., 2018a), we assumed unreabsorbed glucose signals upregulation of SGLT, up to a maximum increase in activity of 30% (Supplemental eqs. S68–S70). Lastly, SGLT2i is assumed to have a weak inhibitory effect on  $\text{Na}^+$  reabsorption through NHE3 (Fu et al., 2014; Pessoa et al., 2014; Coady et al., 2017) (Supplemental eq. S71). We previously showed that 8% inhibition of NHE3 with SGLT2i is sufficient to explain observed electrolyte excretion responses to SGLT2i (Hallow et al., 2018a).

## Technical Implementation

The model was implemented in the open-source programming software R 3.1.2, using the *RxODE* package (Wang et al., 2016). Prior to availability of trial results, simulation results were placed in an online repository at <https://bitbucket.org/hallowkm/dapasalt/src/master/>, which provides time-stamping of the results.

## Virtual Patient Generation

Baseline model parameters are given in Supplemental Tables 1–6. A population of 4000 virtual patients was generated by random sampling of a subset of model parameters over the ranges listed in Table 1. Because the distributions of these parameters within the population are generally unknown, a uniform distribution was used. Parameters to be sampled were chosen based on their mechanistic role of diabetes, kidney injury, and hypertension. Diabetes was simulated by increasing average plasma glucose concentration  $C_{\text{glu}}$  over a range of 7.8–14 mmol/L (corresponding to HbA1c of 6.5%–10.5%). Existing glomerulosclerosis and nephron loss were represented by varying the initial conditions for pressure-induced reductions in glomerular permeability ( $\Delta\text{Perm}$ ) and for nephron loss ( $\Delta\text{nephrons}$ ), respectively. Here, 0% represents no injury, and 100% represents complete loss of glomerular permeability or nephrons, respectively. Podocyte injury ( $\mu_{\text{other,seiv}}$ ) and PT albumin reabsorptive capacity ( $\text{RC}_{\text{albumin}}$ ) were also varied. Ranges for these parameters were chosen such that the resulting proteinuria ranged from 0 to 10 g/day. Hypertension was simulated by varying preafferent and afferent arteriole resistances, PT and collecting duct fractional  $\text{Na}^+$  reabsorption, and pressure natriuresis sensitivity and renal interstitial hydrostatic pressure set point, as previously described (Hallow et al., 2014; Hallow and Gebremichael, 2017a). Sodium intake was also sampled to represent normal population variability in sodium intake. Baseline renin and aldosterone secretion (renin secretion rate, normalized aldosterone

secretion rate) were varied to produce variability in baseline renin and aldosterone concentrations. After simulating to a new steady state, virtual patient values for key clinical measures were compared with physiologically reasonable values, and virtual patients with values falling outside of those ranges were rejected.

## Model Calibration and Validation with Diabetic Nephropathy Clinical Trials

We have previously described calibration and validation of several key model behaviors: 1) We have calibrated the model to describe observed blood pressure reduction and plasma renin changes in response to antihypertensive therapies (ACEi including enalapril, ARBs including losartan, renin inhibitors, thiazide diuretics, and calcium channel blockers) and have shown that it is able to predict the response to combinations of these drugs (Hallow et al., 2014; Hallow and Gebremichael, 2017a). 2) We have shown that the model is able to describe clinically observed changes in urinary glucose, sodium, and volume; changes in plasma sodium and creatinine; and changes in blood pressure in response to SGLT2 inhibition (Hallow et al., 2018a). 3) We previously demonstrated that the model describes progression of albuminuria, hyperfiltration, and GFR decline in murine diabetes models (Mahato et al., 2018). However, the ability of the model to describe the effects of pharmacologic intervention in patients with diabetic nephropathy has not previously been demonstrated. To this end, we simulated several key clinical trials in diabetic nephropathy [RENAAL (Brenner et al., 2001), IDNT (Lewis et al., 2001), NESTOR (Marre et al., 2004), and AVOID (Parving et al., 2008)], focusing on the short-term ( $\leq 6$  months) albuminuria and GFR changes. Over this time period, GFR changes are likely due primarily to renal hemodynamic alterations rather than changes in disease progression (Holtkamp et al., 2011). In this analysis, we did not attempt to predict renal outcomes or long-term changes in GFR.

Each study represents a different segment of the diabetic nephropathy population and/or a different treatment regimen. RENAAL and IDNT investigated ARBs losartan and irbesartan, respectively, in patients with macroalbuminuria and low eGFR. IDNT also required that patients were hypertensive at baseline. NESTOR evaluated the ACEi enalapril in patients with microalbuminuria and moderate eGFR. In these three studies, any prior ACEi or ARB treatment was discontinued before randomization. The AVOID study investigated the addition of the renin inhibitor aliskiren to background ARB (losartan) in patients with macroalbuminuria. However, baseline

TABLE 1  
Parameters varied to produce virtual patients with varying degrees of diabetes, hypertension, and kidney dysfunction

Mechanism	Parameter	Definition	Units	Range	Median	Equation
Diabetic increase in plasma glucose	$C_{\text{glu}}$	Plasma glucose concentration	mM	7.8–14	9.5	3
Glomerulosclerosis	$\Delta\text{Perm}$	Reduction in glomerular permeability	%	0–80	32%	10
Nephron loss	$\Delta\text{nephrons}$	Initial value for nephron loss	%	0–95	51%	2
Podocyte damage due to nonhemodynamic factors	$\mu_{\text{other,seiv}}$	Permanent increase in sieving coefficient	%	0–50	24.7%	12
Variability in PT protein reabsorption	$\text{RC}_{\text{albumin}}$	Proximal tubule capacity for protein reabsorption	pg/min per tubule	1.1–2.1	1.68	6
Variability in aldosterone secretion	$\text{Aldo}_0$	Normalized aldosterone secretion rate	—	0.5–1.5	1	A60
Variability in renin secretion	$\Delta\text{SEC}_{\text{renin},0}$	Change in renin secretion rate	%	–50 to +120	+42%	A52
Variability in sodium intake	$\Phi_{\text{Na},\text{in}}$	Sodium intake rate	mEq/day	80–200	159	A30
Increased renal vascular resistance	$R_{\text{preaff}}$	Preafferent arteriole resistance	mm Hg-min/l	14–26	20	A1
Increased renal vascular resistance	$R_{\text{aff}}$	Afferent arteriole resistance	mm Hg-min/l	10–17	13	A1
Increased PT sodium reabsorption	$\eta_{\text{pt}}$	PT fractional $\text{Na}^+$ reabsorption rate	—	0.6–0.84	0.717	13
Increased collecting duct sodium reabsorption	$\eta_{\text{cd}}$	Collecting duct fractional $\text{Na}^+$ reabsorption rate	—	0.8–0.9	0.85	A14
Reduced sensitivity to pressure natriuresis signals	$S_{\text{P},\text{N}}$	Pressure natriuresis sensitivity	—	0–1	0.5	A50
Altered pressure natriuresis set point	$\text{RIHP}_0$	Renal interstitial hydrostatic pressure set point	mm Hg	9.6–10	9.8	A50

albuminuria was less severe than in RENAAL and IDNT, and baseline eGFR fell between that of RENAAL/IDNT and NESTOR.

RENAAL was used as a calibration study, and model parameters previously calibrated using mouse data (specifically, parameters in eq. 11 defining the relationship between glomerular hydrostatic pressure and protein sieving injury) were refined to improve the fit to the RENAAL UACR data. No other model parameters required adjustment. Then, IDNT, NESTOR, and AVOID were simulated, and results were compared with reported changes in albuminuria and eGFR. It should be noted that although the model calculates GFR directly (eqs. 1 and 2), these studies estimated GFR based on serum creatinine. Equations for estimating GFR are most accurate for GFR less than 60 ml/min.

### Clinical Trial Simulation

For each simulated study, a subset of virtual patients was selected from the full population of virtual patients based on the trial's inclusion and exclusion criteria for HbA1c/blood glucose, UAER or UACR, GFR, and MAP. If more than 70% of patients in the trial were on a background antihypertensive therapy, a run-in period with that therapy was simulated before selecting the trial virtual patients. Controlled sodium intake during a run-in period was modeled when specified in the trial protocol. Treatment with study drug and dose was simulated for the trial duration or for 12 months, whichever was shortest.

### Summary of Calibration/Validation Studies

RENAAL was a randomized, double-blind, placebo-controlled study of losartan in patients with type 2 diabetes (T2D) and nephropathy (UACR > 300 mg/g, serum creatinine 1.3–3 mg/dl) (Brenner et al., 2001; de Zeeuw et al., 2004). If patients were taking ACEi or ARBs at screening, these medications were discontinued and replaced by alternative antihypertensive medications (primarily diuretics and calcium channel blockers). In total, 1513 patients were randomized to 50 mg of losartan or placebo once daily and uptitrated to 100 mg after 4 weeks if blood pressure remained above target levels. The mean follow-up time was 3.4 years. Only changes in UACR and eGFR at 12 months were used in the current analysis.

IDNT was a randomized, double-blind, placebo-controlled study of irbesartan in patients with T2D, hypertension (systolic blood pressure > 135 mm Hg, diastolic blood pressure > 85 mm Hg, or documented treatment with antihypertensive), proteinuria (protein excretion > 900 mg/24 hours), and serum creatinine 1–3 mg/dl in women and 1.2–3 mg/dl in men (Lewis et al., 2001). All ACEi, ARBs, and CCBs (calcium channel blockers) were discontinued for at least 10 days before screening and replaced with other agents. In total, 1715 patients were randomized to irbesartan titrated from 2.5 to 10 mg per day or to placebo. The mean follow-up time was 2.6 years. Only changes in UACR and eGFR at 12 months were used in the current analysis.

NESTOR was a 1-year randomized, double-blind, placebo-controlled study of enalapril or the diuretic indapamine slow release in patients with T2D, microalbuminuria (UAER 28.8–288 mg/day), and hypertension (systolic blood pressure 140–180 mm Hg and diastolic blood pressure < 110 mm Hg) (Marre et al., 2004). All ACEi, ARBs, and CCBs (calcium channel blockers) were discontinued before randomization. In total, 570 patients were randomized to one of three groups: enalapril 10 mg, indapamine 1.5 mg sustained release, or placebo.

AVOID was a 6-month randomized, double-blind, placebo-controlled study of aliskiren added to 100 mg of losartan in patients with T2D and macroalbuminuria (UACR > 300 mg/g) (Lewis et al., 2001). Inclusion criteria included eGFR > 30 ml/min per 1.73 m<sup>2</sup> and serum creatinine 1–3 mg/dl in women and 1.2–3 mg/dl in men. During a 3-month run-in period, all RAAS blockers were discontinued and replaced with 100 mg losartan daily, plus additional antihypertensives as needed to achieve target blood pressure of <130/80 mm Hg.

In total, 599 patients were randomized to aliskiren (150 mg uptitrated to 300 mg at 12 weeks) or to placebo.

**DAPASALT Study Protocol.** DAPASALT is an open label, mechanistic, three-arm study to evaluate the natriuretic effect of 2 weeks of dapagliflozin treatment with participants on a fixed sodium diet. The study population consists of three groups of patients (Caucasians, age 18–75 years of age) with either 1) T2D without renal impairment (HbA1c 6.5%–10%, eGFR 90–130 ml/min per 1.73 m<sup>2</sup>), 2) T2D with impaired renal function (HbA1c 6.5%–10%, eGFR 25–50 ml/min per 1.73 m<sup>2</sup>), or 3) normoglycemic individuals with impaired renal function (eGFR 25–50 ml/min per 1.73 m<sup>2</sup>) and confirmed diagnosis of focal segmental glomerular sclerosis, IgA, or membranous glomerular nephropathy. For inclusion, patients must also have been treated with an ARB for at least 6 weeks prior to starting the trial, and for the individuals with T2D, a stable dose(s) of appropriate glucose-lowering medications other than SGLT2i must be present. Patients must also have stable urinary sodium excretion on two successive 24-hour measures during the run-in period. Patients with systolic and diastolic blood pressure above 160/110 mm Hg, respectively, were excluded. Full inclusion and exclusion criteria are included in the Supplemental Material. The study aims to enroll 51 patients, 17 per arm, to ensure that 15 patients complete each arm. A 2-week screening and run-in period precedes the active treatment period, and patients receive standardized meals with a sodium content of 150 mmol/day starting at 6 days before treatment and continuing through the study. Subjects receive 10 mg pf dapagliflozin daily for 14 days, followed by a 4-day washout period. The washout period was not considered in the analysis presented here. Study endpoints are given in Table 2. Plasma volume will be measured by indocyanine green distribution, and extracellular fluid volume will be measured by bioimpedance spectroscopy analysis.

## Results

**Virtual Patient Population.** Of the 4000 potential virtual patients generated, 3389 had physiologically reasonable steady-state values (MAP 70–160 mm Hg, GFR 15–150 ml/min, UAER 0–10,000 mg/day) and were considered acceptable. As shown in Fig. 2, top row, the distributions of baseline GFR, MAP, and UACR in the acceptable virtual patient population covered a wide range, providing a sufficient population from which to sample clinical trial populations. UAER was lognormally distributed, and GFR and MAP were normally distributed. Table 3 summarizes the number of microalbuminuric, macroalbuminuric, and hypertensive virtual patients within each GFR category. Figure 3 illustrated the effect of virtual patient differences in nephron number, glomerulosclerosis, and blood glucose on baseline GFR and UAER. As expected, GFR was lower and SNGFR was higher in virtual patients with greater nephron loss. Virtual patients with higher glomerulosclerosis tended to have lower GFR, although some virtual patients had low GFR with minimal glomerulosclerosis. Blood glucose was not associated with GFR. UAER increased with moderate nephron loss, but it decreased again as nephron loss increased further. UAER tended to be higher in virtual patients with more glomerulosclerosis, and there was no association between blood glucose and UAER.

To replicate trials in which patients were on an ARB therapy at baseline (AVOID and DAPASALT), virtual patients were simulated on an ARB to reach a new baseline. As shown in Fig. 2, bottom row, this shifted the virtual population distributions of UAER, GFR, and MAP to the left, but the full range of each variable was still covered.

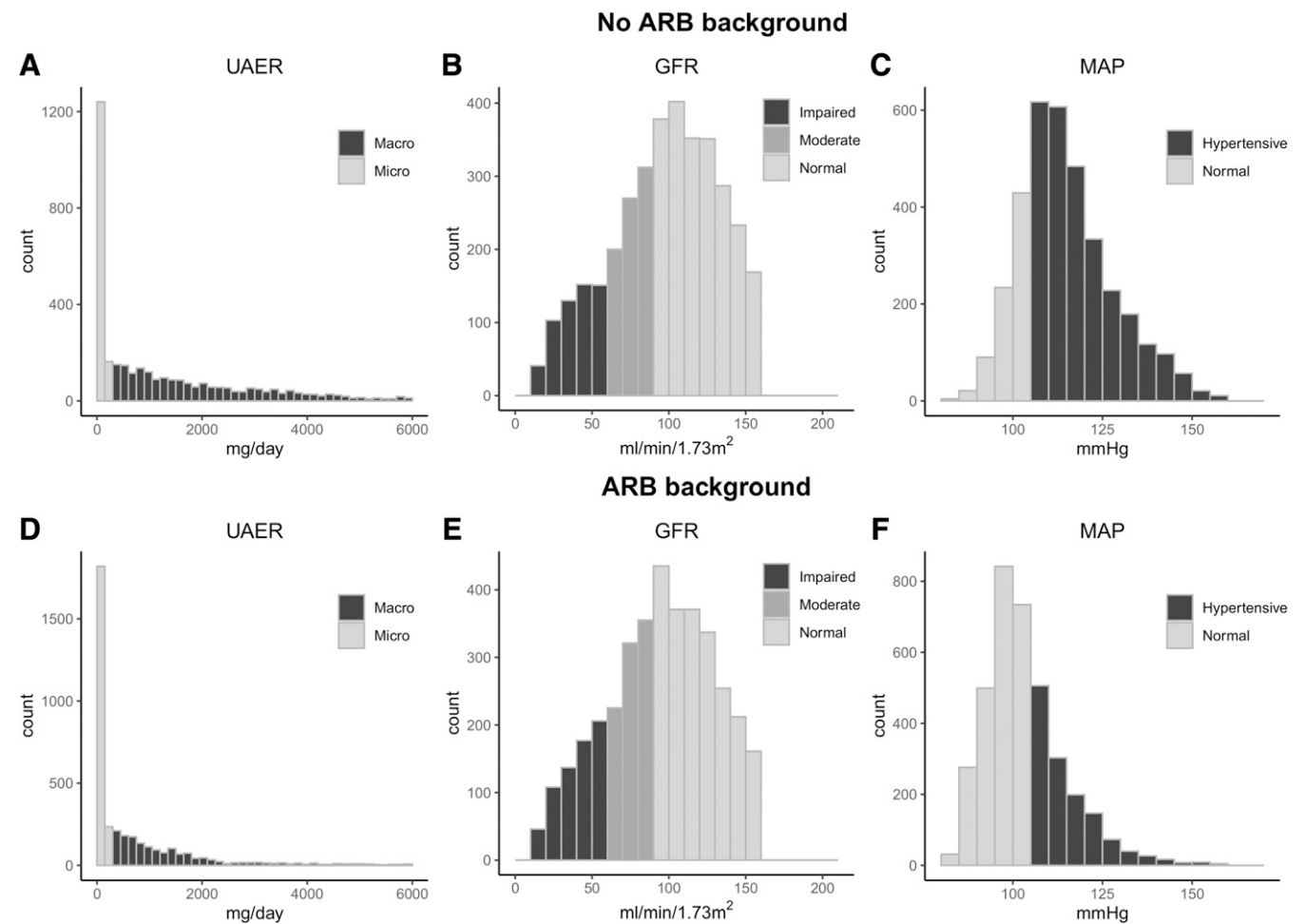


TABLE 2  
Primary and secondary endpoints of the DAPASALT study

Variable	Type	Measure	Time Points
24-h sodium excretion	Primary	Change in mean	Baseline vs. mean of days 2–4
	Secondary		Baseline vs. mean of days 12–14
	Secondary		Days 12–14 vs. days 15–17
24-h sodium excretion	Secondary	Change in mean	Baseline vs. day 4
24-h sodium excretion			Baseline vs. day 13
24-h systolic blood pressure			Day 13 vs. day 17
24-h systolic blood pressure			
24-h systolic blood pressure			
Plasma volume	Secondary	Change in mean	Baseline vs. Day 4
			Baseline vs. Day 14
			Day 14 vs. Day 17
Extracellular fluid volume	Secondary	Change in mean	Baseline vs. Day 14

**Calibration and Validation: Simulation of Previous Diabetic Nephropathy Clinical Trials.** After selecting study populations from the larger virtual population by applying each trial’s inclusion/exclusion criteria for albuminuria and eGFR, the virtual study populations produced were reasonably representative of the clinically reported baseline albuminuria and eGFR measures in each study (Fig. 4, top row). There was heterogeneity across studies in albuminuria measurement used (UACR or UAER) and statistic reported

(geometric mean or median, S.D., interquartile range, or 95% confidence interval), and we did not explicitly try to fit these values. The simulated response for each trial also reproduced the reported reductions in albuminuria and eGFR. For RENAAL, model parameters were optimized to fit the observed albuminuria response. For the remaining studies, the model-predicted response reasonably reproduced the observed changes in albuminuria and eGFR. One exception to this was the AVOID



**Fig. 2.** (A–C) Virtual patient population covers the physiologic range of baseline UAER, GFR, and MAP. (D–F) After run-in on an ARB (losartan, 100 mg), baseline distributions are leftward-shifted but still cover a wide range.

TABLE 3

Prevalence of albuminuria and hypertension in virtual patient population by renal function status

Renal Function	Microalbuminuria	Macroalbuminuria	Hypertensive
Impaired, GFR < 60 ml/min ( <i>n</i> = 592)	43.4%	58.0%	83%
Moderate impairment, GFR 60–90 ( <i>n</i> = 794)	53.4%	46.5%	71.6%
Normal, GFR > 90 ml/min ( <i>n</i> = 2003)	61.1%	38.9%	68.6%

GFR response. This study showed a placebo-adjusted increase in eGFR—a finding that is inconsistent with a considerable body of studies showing reductions in eGFR with RAAS blockade, both alone and in combination (Mann et al., 2008; Holtkamp et al., 2011). However, it should be noted that the model does not reproduce this unexpected behavior.

**Prospective Simulation of DAPASALT.** Figure 5 shows the virtual study populations for each arm in DAPASALT. The arms for T2D with preserved renal function, T2D with impaired renal function, and normoglycemic with impaired renal function will be referred to here as D-PRF, D-IRF, and N-IRF. There were no inclusion/exclusion criteria for UAER. Although each arm of the DAPASALT study will include 15–17 subjects, a larger number of virtual patients were included in the virtual population to allow the model to capture the full range of responses that might be observed.

Figures 6–8 show the simulated time course of key endpoints measured in the study for each of the three study arms, and Fig. 9 compares the response between the three groups at key time points. The washout period was not simulated. As

expected, predicted 24-hour UGE is highest in the D-PRF group, lower in D-IRF, and lowest in N-IRF (median 94.6, 35.9, and 19.7 g/day on day 14, respectively). In all groups, 24-hour Na<sup>+</sup> excretion is predicted to peak on day 1, overcompensate and dip just below baseline on day 2, and then quickly return to baseline as the virtual patients again reached Na<sup>+</sup> balance. Water excretion is also predicted to peak on day 1, but it subsequently normalizes more slowly than Na<sup>+</sup> excretion. In addition, water excretion is predicted to take longer to return to baseline in renally impaired groups (around day 14) compared with the normal renal function group (around day 7).

Urinary Na<sup>+</sup> and water excretion are not in parallel because urinary Na<sup>+</sup> excretion reflects changes in proximal tubule Na<sup>+</sup> reabsorption, whereas water excretion reflects changes in both proximal tubule and the distal nephron. Compensatory mechanisms eventually restore both Na<sup>+</sup> and water balance, but mechanisms regulating Na<sup>+</sup> balance (e.g., renin, pressure natriuresis) achieve balance more quickly than mechanisms regulating water balance (mainly vasopressin).

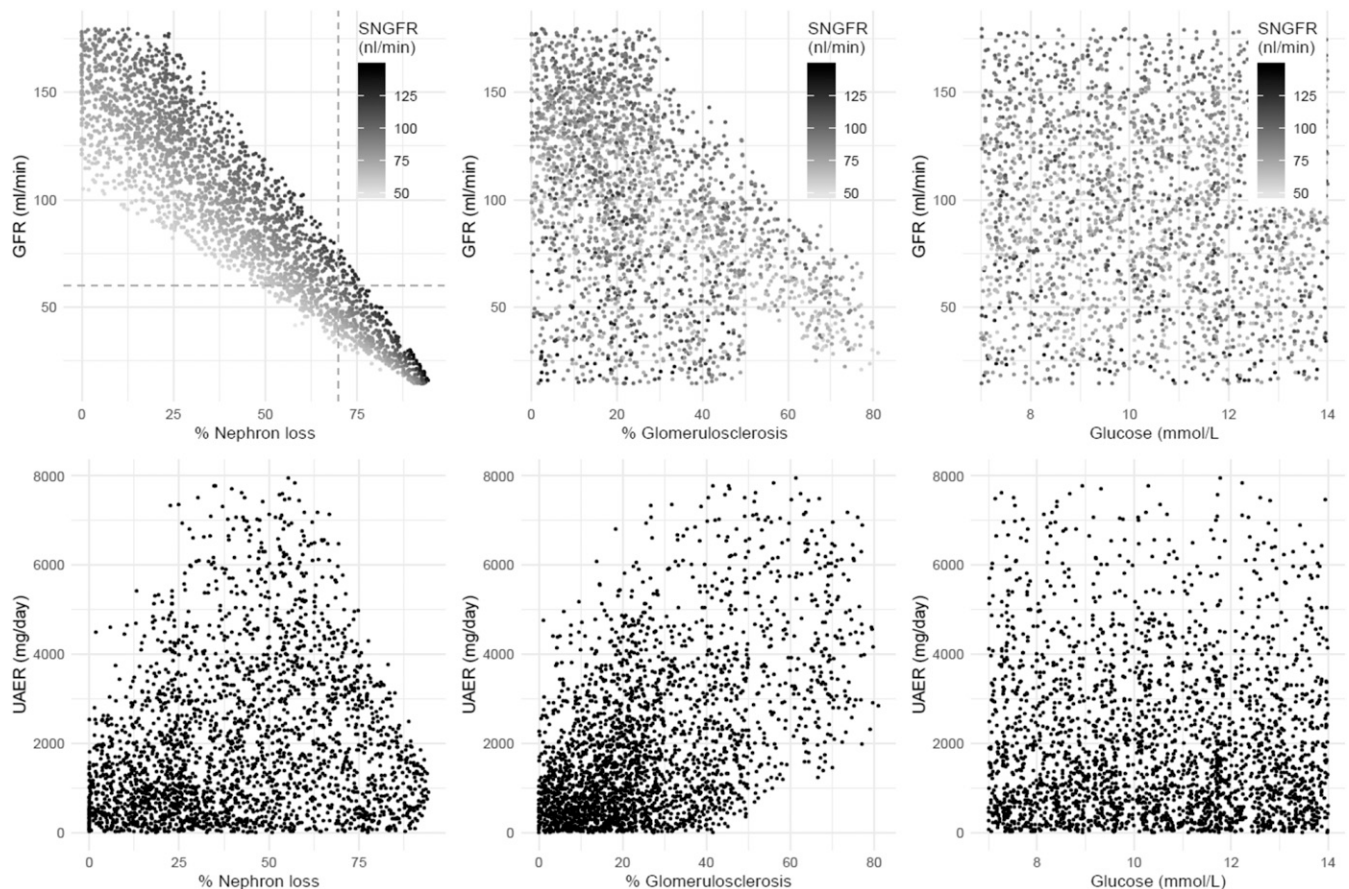


**Fig. 3.** Effect of virtual patient parameter values on baseline GFR and UAER.



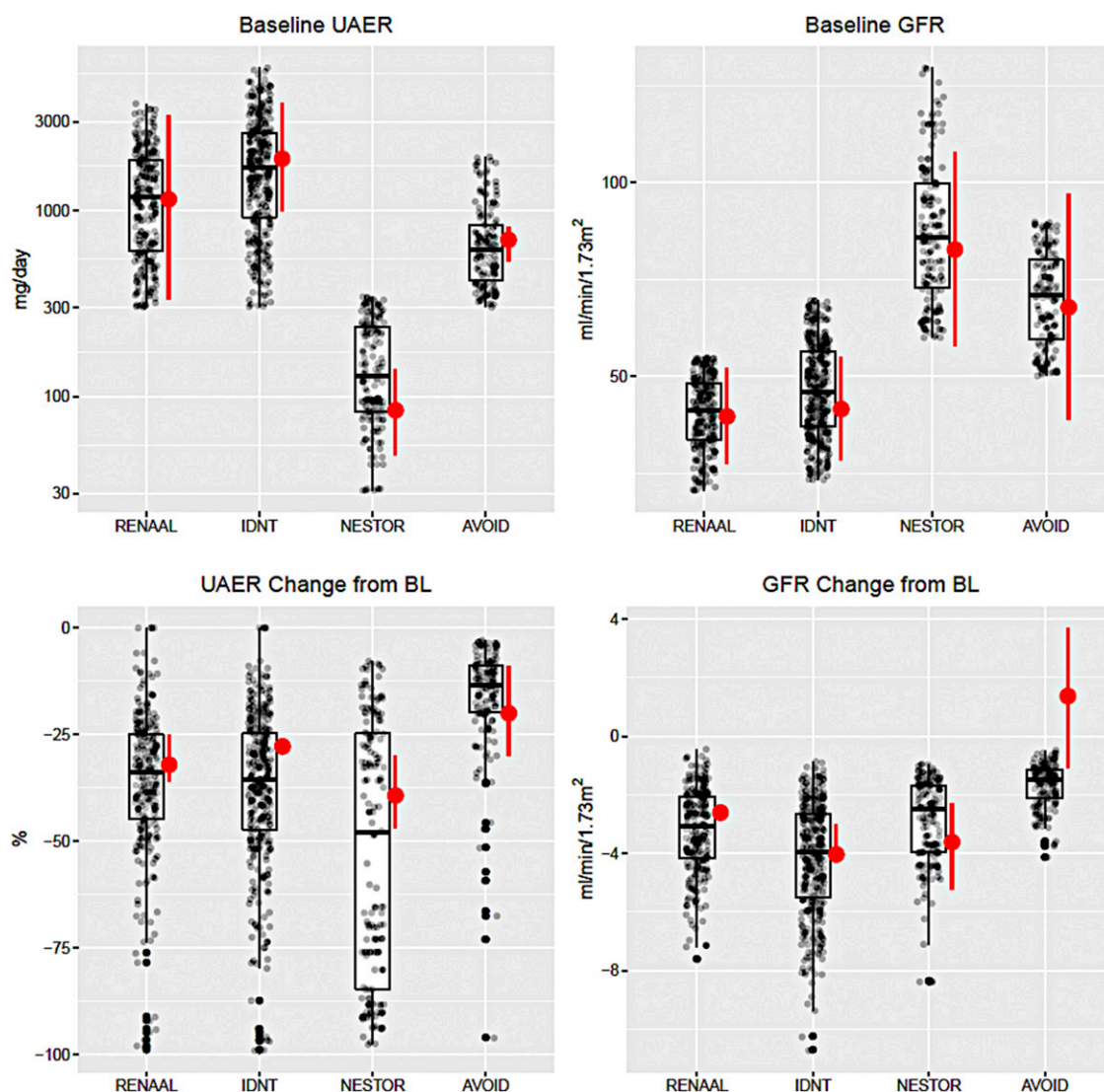


**Fig. 4.** Simulated and observed baseline (top row) and change from baseline (bottom row) in GFR/eGFR and UAER of key diabetic nephropathy clinical trials. Boxes: simulated median and interquartiles; gray circles: individual virtual patients; red: clinical study reported values. (RENAAL (Brenner et al., 2001): UAER is geometric mean  $\pm$  S.D.; IDNT (Lewis et al., 2001): UAER median and interquartile range, no measure of variability reported for change in UAER; NESTOR (Marre et al., 2004): UAER geometric mean and interquartile range; AVOID (Parving et al., 2008): UAER geometric mean and 95% confidence interval. For all studies, eGFR is mean  $\pm$  S.D.. No S.D. reported for RENAAL change in eGFR.)

The decrease in MAP in D-PRF is predicted to be slightly larger than in the D-IRF group ( $-5.1$  vs.  $-3.6$  mm Hg). MAP reduction in the N-IRF group is predicted to be small (1 mm Hg).

Our simulations predict that the initial reduction in GFR will be much smaller in the impaired renal function groups ( $-3.8$  and  $-2.3$  ml/min in D-IRF and N-IRF groups, respectively) compared with the D-PRF group ( $-15.2$  ml/min). The initial reduction in GFR also varied widely within the D-PRF group, as indicated by the width of the interquartile range (Fig. 6). Further analysis showed that the largest drops occurred in hyperfiltering virtual patients (baseline GFR  $> 110$  ml/min, analysis not shown).

UAER is predicted to decrease substantially in all three groups. In patients with diabetes, the UAER reduction is predicted to be less but still quite large in the impaired renal function group (34.8%) compared with the normal renal function group (45.8%). A smaller reduction (14.2%) is predicted in the N-IRF group. Our simulations predict that the maximum UAER reduction will occur within 14 days.

As we have modeled previously, reductions in IFV are predicted to be much greater than reductions in blood volume. Predicted blood volume reduction is largest in the D-PRF (210 ml), smaller in D-IRF (150 ml), and smallest in the N-IRF group (40 ml). On the other hand, predicted IFV reduction is larger in the D-IRF group than in the D-PRF group (1.81 vs. 1.68 l) and was still substantially reduced in the N-IRF group (1 l). Thus, the ratio of IFV to blood volume reduction is predicted to be larger in the renal impairment groups than in normal renal function.

## Discussion

**Clinical Implications of Model Predictions.** Given the weaker glycosuria response to SGLT2i in patients with renal impairment and in nonpatients with diabetes, volume changes resulting from osmotic diuresis with SGLT2i might be expected to be diminished in these populations. However, the model predicts IFV reduction will be similar in T2D with

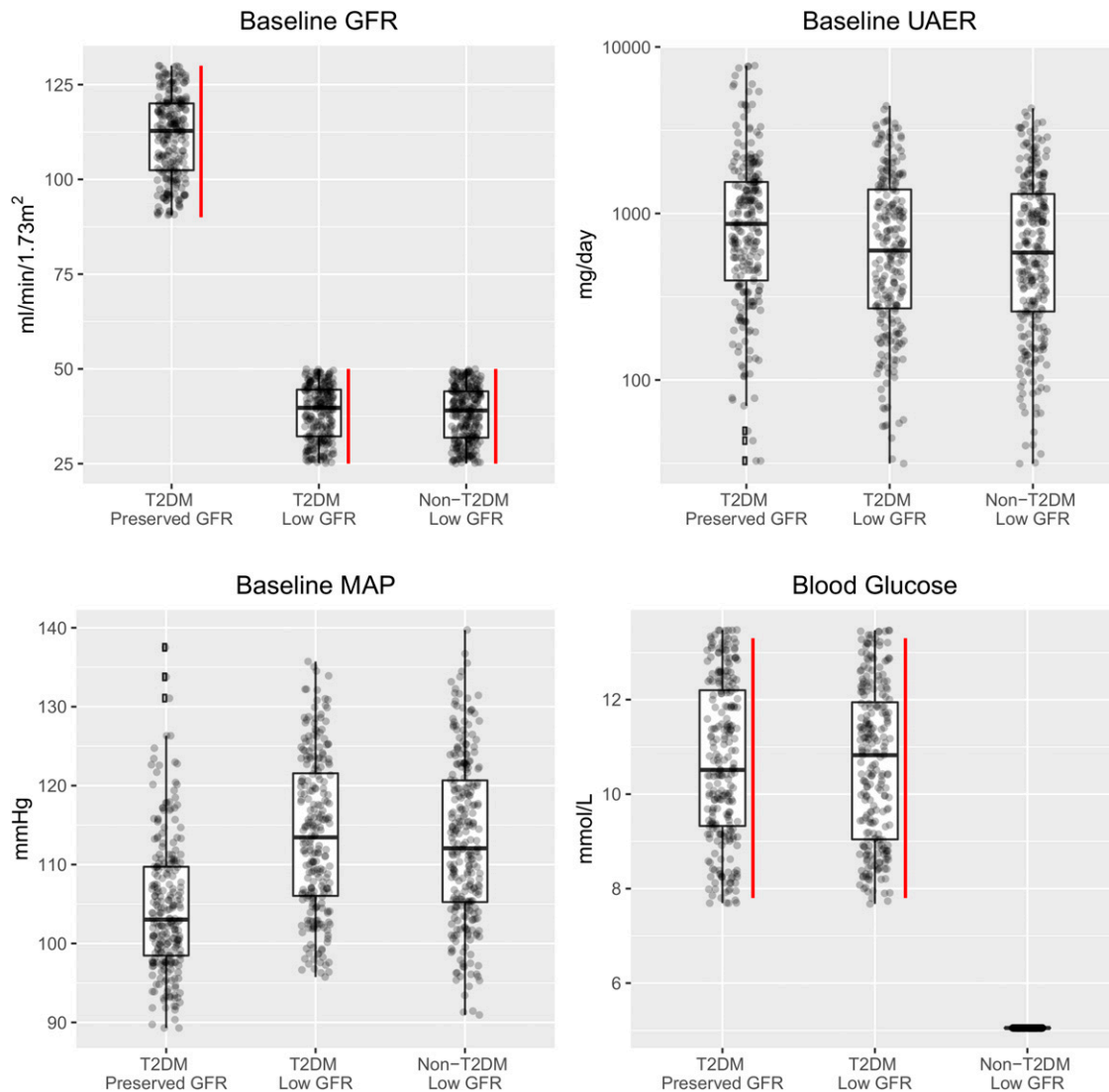


**Fig. 5.** Baseline characteristics of DAPASALT virtual study arms (T2DM preserved GFR  $n = 250$ , T2DM low GFR  $n = 250$ , non-T2DM low GFR  $n = 272$ ). Red bars: study inclusion/exclusion criteria.

and without renal impairment and that nondiabetics with renal impairment will see smaller but still substantial IFV reductions, even with much lower UGE. Assuming IFV plays an important role in the cardiovascular benefits of SGLT2i, this is consistent with recent findings of the DAPA-HF (Dapagliflozin in Patients with Heart Failure and Reduced Ejection Fraction) study, in which significant improvements in the primary endpoint (worsening of heart failure or cardiovascular death) were seen across all baseline GFRs and independent of diabetic status (McMurray et al., 2019).

The model also suggests a mechanistic explanation for these predictions. Within a single nephron, predicted changes in water excretion were similar between D-PRF and D-IRF groups. However, because the D-PRF have more functioning nephrons, the initial peak in water excretion in this group was larger (Fig. 6). The modeling suggests this causes a larger vasopressin response, which limits further excretion and quickly returns water excretion to baseline. In D-IRF, the predicted initial water excretion and thus vasopressin response is lower, so compensation occurs more slowly, allowing

similar total water excretion and thus similar volume changes as in the D-PRF group, even though the initial peak was smaller.

A second finding, which we demonstrated previously in single virtual patients (Hallow et al., 2018a), is that glomerular hydrostatic pressure reductions, which likely play a large role in dapagliflozin's renoprotective effects, are predicted to be similar in patients with normal or impaired renal function, and initial GFR drop is expected to be smaller in impaired renal function. The sustained glomerular pressure reduction likely explains why the antiproteinuric effects are sustained in patients with low GFR (Heerspink et al., 2016; Fioretto et al., 2018).

**Comparison with Available Data.** Although DAPASALT study results are not yet available, several available data support the predicted responses. Our simulations reproduce higher UGE observed in patients with normal versus impaired renal function (List et al., 2009; Kohan et al., 2014). Predicted MAP reductions of 3–5 mm Hg are consistent with previous studies (List et al., 2009; Wilding et al., 2009;

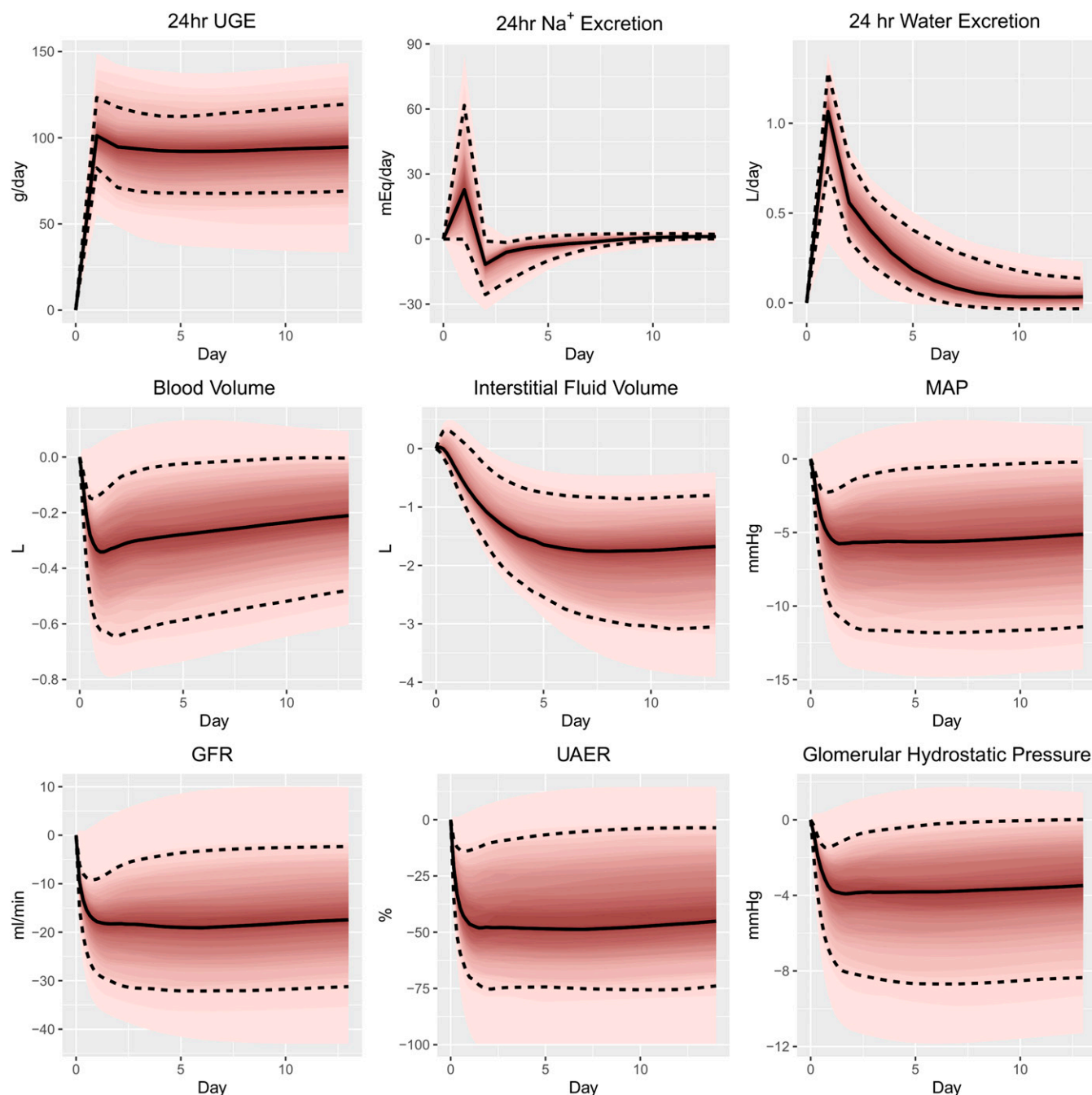


**Fig. 6.** DAPASALT D-PRF arm. Simulated time course for change from baseline with 10 mg dapagliflozin. Solid line: median; dashed lines: 25%–75%; pink bands: 0%–100% range of response.

Ferrannini et al., 2010). The simulations reproduce the well known initial drop in GFR with SGLT2i initiation. This reversible initial reduction is followed by a much slower rate of GFR decline (Wanner et al., 2016). Our simulations predict the initial GFR drop with dapagliflozin will be smaller in D-IRF than D-PRF. The predicted magnitude in D-IRF (−3.8 ml/min) is consistent with reported eGFR changes in clinical studies of diabetic chronic kidney disease (CKD). In the DERIVE study, in patients with T2D with stage 3a CKD treated with dapagliflozin, GFR fell by 5 ml/min per 1.73 m<sup>2</sup> at week 4 (Fioretto et al., 2018). A similar reduction (−4 ml/min per 1.73 m<sup>2</sup>) was observed with canagliflozin at week 6 in T2D

with stage 3 CKD (Yamout et al., 2014). Another small study in patients with more severe CKD (mean eGFR 30.3 ml/min per 1.73 m<sup>2</sup>) found a smaller (1.3 ml/min per 1.73 m<sup>2</sup>) reduction. This is consistent with our predicted smaller initial GFR reduction in patients with lower baseline GFR.

Most studies reporting renal function changes with SGLT2i have used serum creatinine to estimate GFR, although a few used inulin clearance or other methods to measure GFR directly. eGFR is accurate for GFR less than 60 ml/min per 1.73 m<sup>2</sup> but may be less accurate for higher GFRs. Studies reporting eGFR changes in patients without renal impairment have reported reductions of 4 to 5 ml/min per 1.73 m<sup>2</sup>

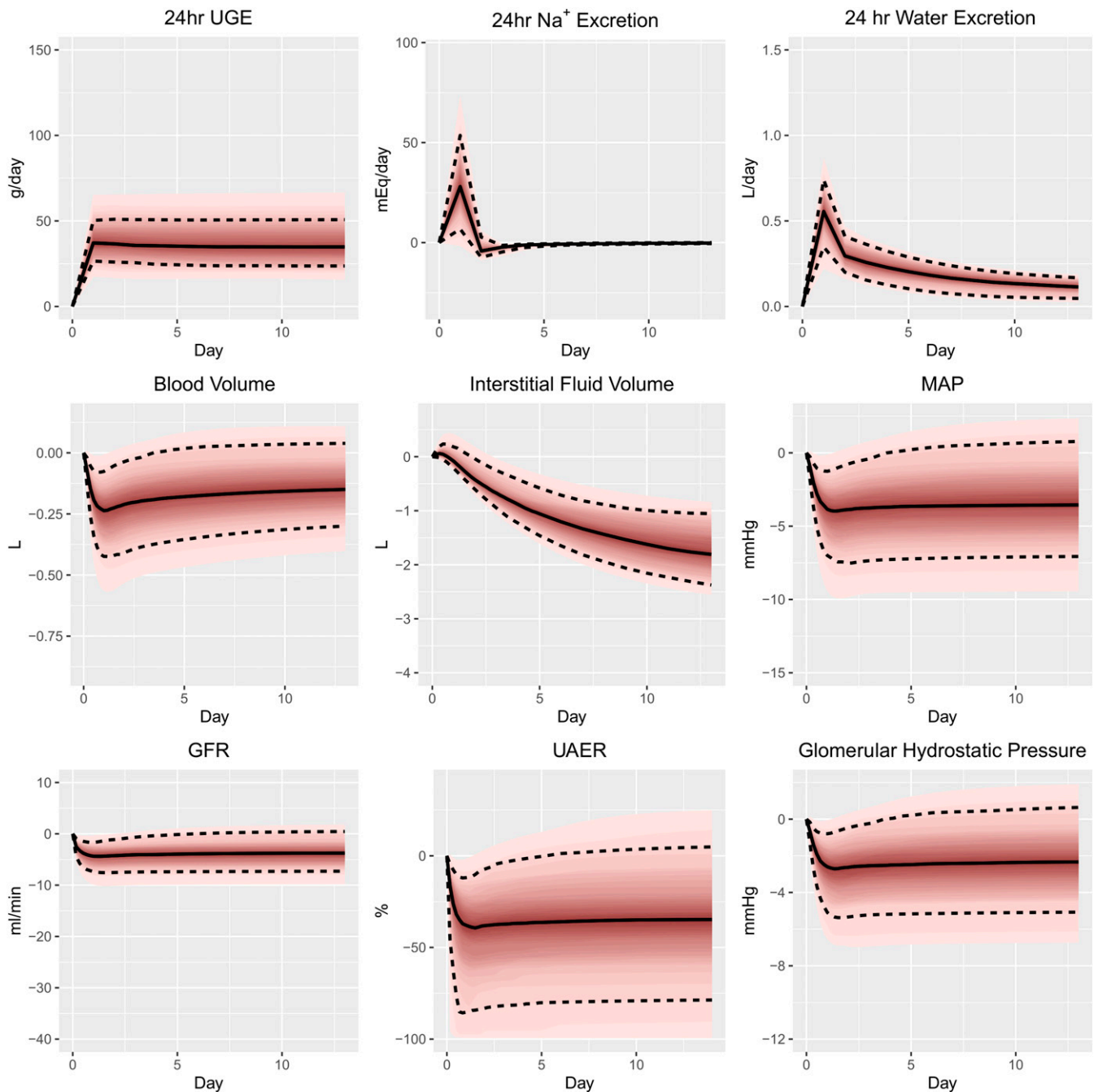


**Fig. 7.** DAPASALT D-IRF arm. Simulated time course for change from baseline with 10 mg dapagliflozin. Solid line: median; dashed lines: 25%–75%; pink bands: 0%–100% range of response.

(Heerspink et al., 2016), and pooled analyses have shown no dependence of change in eGFR on baseline eGFR (Pettykiv et al., 2017). However, studies that measured GFR directly have found larger reductions. In one study, GFR dropped by 10.8 ml/min initially in patients with T2D and normal renal function treated with dapagliflozin (Lambers Heerspink et al., 2013). Another study reported reductions of 5, 10, and 12 ml/min in fasted, euglycemic, and hyperglycemic states, respectively (van Bommel et al., 2020). Cherney et al. (2014) found that empagliflozin reduced GFR in hyperfiltering patients with type 1 diabetes by 25–45 ml/min per 1.73 m<sup>2</sup>, depending on glycemic state. They found no GFR change in nonhyperfiltering patients.

The magnitude of changes predicted in the DAPASALT D-PRF group (–15.2 ml/min) are consistent with studies measuring GFR directly, and it is possible that measured changes in eGFR in DAPASALT may underpredict true changes in GFR. Our simulations are also consistent with a larger initial GFR drop in hyperfiltering than nonhyperfiltering patients.

The model-predicted changes in albuminuria are consistent with studies showing consistent proteinuria reduction with SGLT2i. In patients with T2D and moderate renal function (baseline eGFR of 72–82 ml/min per 1.73 m<sup>2</sup>), 10 mg dapagliflozin reduced UACR by 45% at week (Heerspink et al., 2016) and reduced 24-hour UAER by 36.2% at 6 weeks (Pettykiv



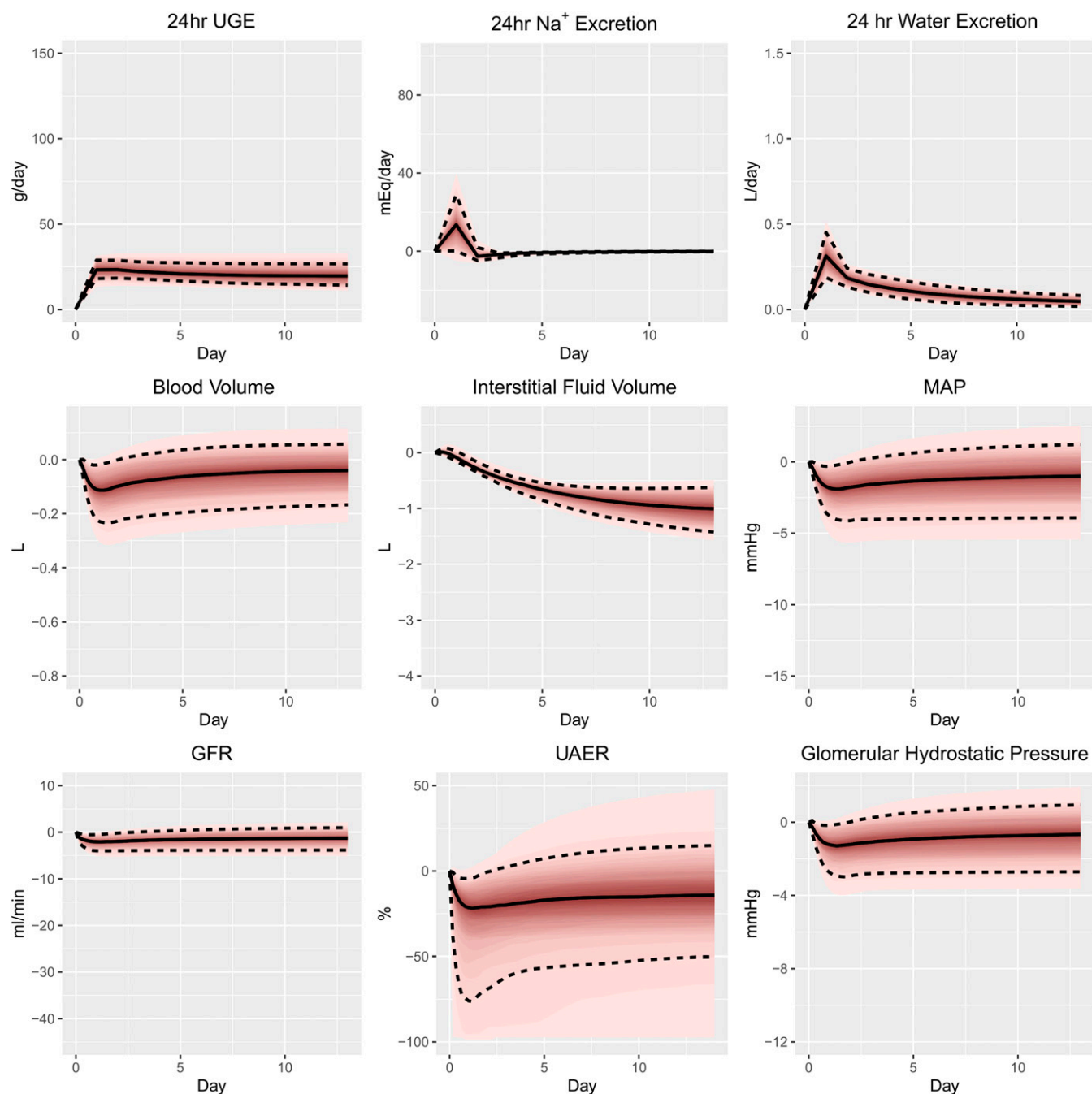


**Fig. 8.** DAPASALT N-IRF arm. Simulated time course for change from baseline with 10 mg dapagliflozin. Solid line: median; dashed lines: 25%–75%; pink bands: 0%–100% range of response.

et al., 2017). In T2D patients with stage 3a CKD and albuminuria, UACR fell 30.7% at week 4 and 41.7% by week 12 (Fioretto et al., 2018), whereas in stage 3b–4 CKD, UACR was reduced 38.4% over 102 weeks. Our predicted reductions of 45% and 35% in T2D with normal and impaired renal function, respectively, are consistent with these findings.

Fewer data are available on fluid volume changes with SGLT2i. As we predict here and in previous analyses of single virtual patients (Hallow et al., 2018a,b), SGLT2i may elicit much larger relative reductions in IFV than in blood volume. This decongestive effect without excessive reduction in blood pressure and organ perfusion may explain the unexpectedly

large benefits on heart failure (Zinman et al., 2015; McMurray et al., 2019). To our knowledge, DAPASALT will be the first to measure changes in both IFV and blood volume in the same study. However, studies have separately reported measures that reflect blood or total extracellular fluid volume change. SGLT2i have consistently been found to increase hematocrit, suggesting blood volume reduction. Hematocrit increases of 1.3% and 2.2% were reported in T2D with normal renal function (Lambers Heerspink et al., 2013; Wada et al., 2019). If red blood cell volume remains constant, the model-predicted changes in blood volume correspond to 1.7% hematocrit increase in T2D with preserved GFR, consistent with these

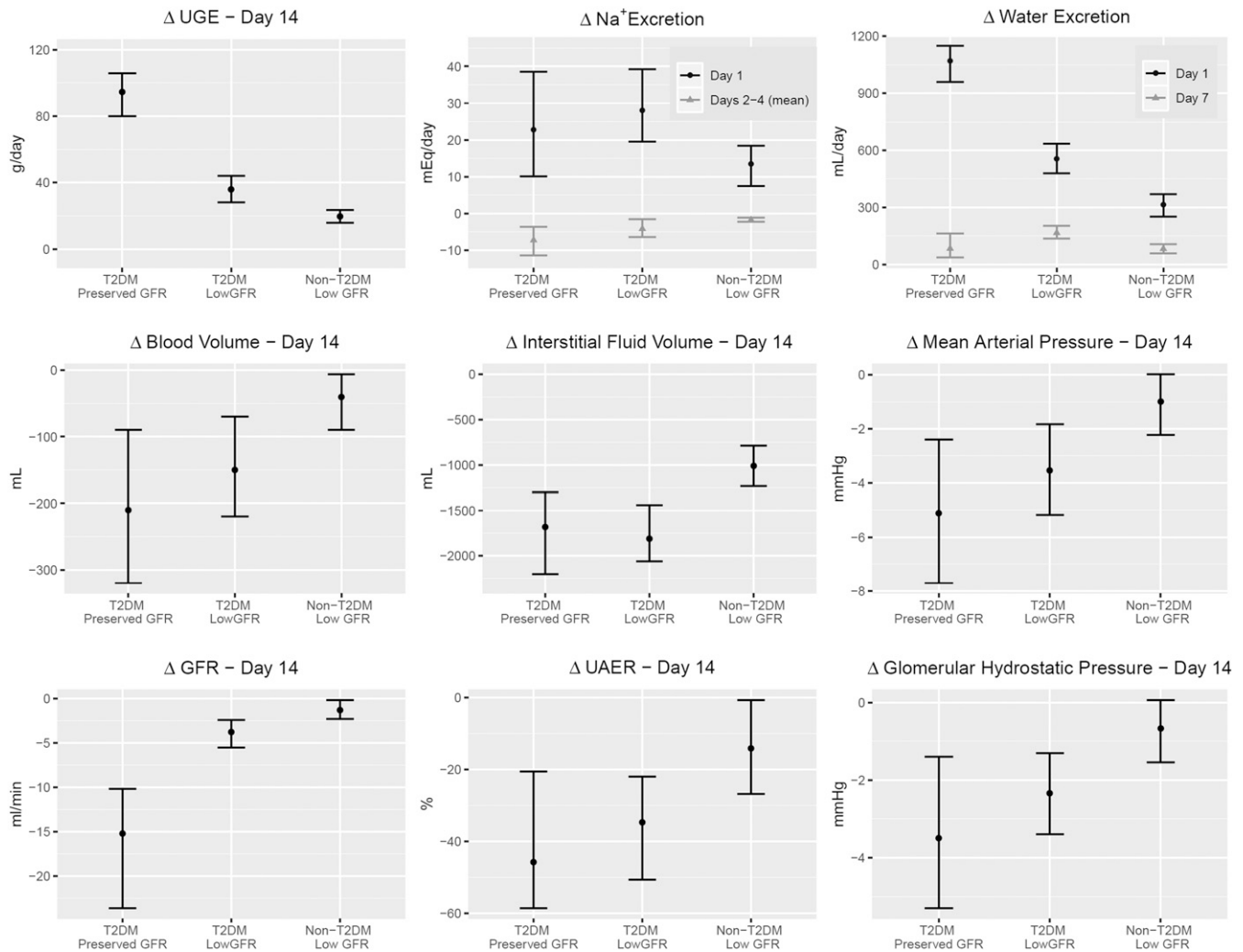


**Fig. 9.** Simulated response to daily dosing of 10 mg dapagliflozin in DAPASALT study arms. All data are medians and interquartile ranges.

studies. Hematocrit changes may also reflect changes in hematopoiesis (Maruyama et al., 2019), but these effects were not modeled here. Two recent studies used bioimpedance to measure extracellular water changes. Unfortunately, these studies did not report hematocrit, so relative reductions in blood and interstitial volumes cannot be determined. These studies were nonrandomized and were not placebo-controlled and thus should be interpreted with care. In Ohara et al. (2019), extracellular water was reduced by 8.4% in patients with diabetes with impaired renal function treated with dapagliflozin, and our simulations predict a 9.5% reduction. A recent observational study in T2D with normal renal function treated with empagliflozin or dapagliflozin reported a smaller reduction (400 mL/1.73 m<sup>2</sup>) at day 3. A third study with tofogliflozin showed a 0.3-kg reduction in extracellular water (Kamei et al., 2018). This study actually showed a non-significant hematocrit decrease, inconsistent with other studies consistently showing increases.

**Model Validation.** Models cannot reproduce all aspects of physiology and disease. Making predictions and comparing with clinical data are ways to determine whether the model is “good enough” or whether important mechanisms are missing. We previously showed that the model reproduces biomarker

and blood pressure responses to RAAS blockers, diuretics, and calcium channel blockers in hypertension (Hallow et al., 2014) and urinary and serum biomarker responses to dapagliflozin in normal subjects (Hallow et al., 2018a). Here, we further retrospectively validated the kidney injury and albuminuria components of the model by demonstrating reasonable agreement between model predictions and observed changes in albuminuria and eGFR for previous diabetic nephropathy clinical trials. This validation demonstrated that the renal physiology/pathophysiology/pharmacology represented in the model is sufficient for describing responses in this population and provides confidence for making prospective predictions in similar populations treated with SGLT2i.

**Limitations.** The model captures some but not all sources of variability in SGLT2i response. Thus, predicted interquartile ranges are likely narrower than true interquartile ranges. DAPASALT virtual patients were selected based on inclusion/exclusion criteria. Because we do not know the true baseline characteristics, virtual and real populations may differ. In particular, because no limits were placed on UACR in the DAPASALT protocol, virtual and real baseline UACR could be quite different, which could impact predicted treatment responses. Few studies report time courses for albuminuria



changes prior to 4 weeks. If the model overestimates the speed of UAER reduction, the 2-week UAER response may be overpredicted. For the normoglycemic arm, we did not distinguish between mechanisms of IgA nephropathy, focal segmental glomerular sclerosis, or membranous glomerular nephropathy. Once study results are available, comparison of simulated and observed baseline characteristics and responses may provide further information for better modeling these populations.

## Conclusions

The model predicts similarly large IFV reduction between D-PRF and D-IRF and less, but still substantial, IFV reduction in N-IRF, even though glycosuria is attenuated in groups with impaired renal function. When DAPASALT results become available, comparison with these prospective simulations will provide a basis for evaluating how well we understand the renal and volume homeostasis mechanism(s) of SGLT2i. If the prospective simulations predict the results well, this will also provide further validation of the model as a tool for future predictions.

## Authorship Contributions

*Participated in research design:* Hallow, Boulton, Penland, Helmlinger, Nieves, Heerspink, Greasley.

*Conducted Experiments:* Hallow, Nieves.

*Contributed new reagents or analytic tools:* Hallow.

*Performed data analysis:* Hallow, Nieves.

*Wrote or contributed to the writing of the manuscript:* Hallow, Boulton, Penland, Helmlinger, van Raalte, Heerspink, Greasley.

## References

- Bivona BJ, Park S, and Harrison-Bernard LM (2011) Glomerular filtration rate determinations in conscious type II diabetic mice. *Am J Physiol Renal Physiol* **300**: F618–F625.
- Brenner BM, Cooper ME, de Zeeuw D, Keane WF, Mitch WE, Parving HH, Remuzzi G, Snapinn SM, Zhang Z, and Shahinfar S; RENAAL Study Investigators (2001) Effects of losartan on renal and cardiovascular outcomes in patients with type 2 diabetes and nephropathy. *N Engl J Med* **345**:861–869.
- Cherney DZ, Perkins BA, Soleymanlou N, Maione M, Lai V, Lee A, Fagan NM, Woerle HJ, Johansen OE, Broedl UC, et al. (2014) Renal hemodynamic effect of sodium-glucose cotransporter 2 inhibition in patients with type 1 diabetes mellitus. *Circulation* **129**:587–597.
- Coady MJ, El Tarazi A, Santer R, Bissonnette P, Sasseville LJ, Calado J, Lussier Y, Dumayne C, Bichet DG, and Lapointe JY (2017) MAP17 is a necessary activator of renal Na<sup>+</sup>/glucose cotransporter SGLT2. *J Am Soc Nephrol* **28**:85–93.
- Dekkers CCJ, Petrykiv S, Laverman GD, Cherney DZ, Gansevoort RT, and Heerspink HJL (2018) Effects of the SGLT-2 inhibitor dapagliflozin on glomerular and tubular injury markers. *Diabetes Obes Metab* **20**:1988–1993.
- de Zeeuw D, Remuzzi G, Parving HH, Keane WF, Zhang Z, Shahinfar S, Snapinn S, Cooper ME, Mitch WE, and Brenner BM (2004) Proteinuria, a target for renoprotection in patients with type 2 diabetic nephropathy: lessons from RENAAL. *Kidney Int* **65**:2309–2320.
- Ferrannini E, Ramos SJ, Salsali A, Tang W, and List JF (2010) Dapagliflozin monotherapy in type 2 diabetic patients with inadequate glycemic control by diet and exercise: a randomized, double-blind, placebo-controlled, phase 3 trial. *Diabetes Care* **33**:2217–2224.
- Fioretto P, Del Prato S, Buse JB, Goldenberg R, Giorgino F, Reyner D, Langkilde AM, Sjöström CD, and Sartipy P; DERIVE Study Investigators (2018) Efficacy and safety of dapagliflozin in patients with type 2 diabetes and moderate renal impairment (chronic kidney disease stage 3A): the DERIVE Study. *Diabetes Obes Metab* **20**:2532–2540.
- Fioretto P, Giaccari A, and Sesti G (2015) Efficacy and safety of dapagliflozin, a sodium glucose cotransporter 2 (SGLT2) inhibitor, in diabetes mellitus. *Cardiovasc Diabetol* **14**:142.
- Flyvbjerg A, Dagnaes-Hansen F, De Vriese AS, Schrijvers BF, Tilton RG, and Rasch R (2002) Amelioration of long-term renal changes in obese type 2 diabetic mice by a neutralizing vascular endothelial growth factor antibody. *Diabetes* **51**:3090–3094.
- Fu Y, Gerasimova M, Mayoux E, Masuda T, and Vallon V (2014) SGLT2 inhibitor empagliflozin increases renal NHE3 phosphorylation in diabetic Akita mice: possible implications for the prevention of glomerular hyperfiltration (Abstract). *Diabetes* **63**:132.
- Guthrie R (2018) Canagliflozin and cardiovascular and renal events in type 2 diabetes. *Postgrad Med* **130**:149–153.
- Hallow KM and Gebremichael Y (2017a) A quantitative systems physiology model of renal function and blood pressure regulation: application in salt-sensitive hypertension. *CPT Pharmacometrics Syst Pharmacol* **6**:393–400.
- Hallow KM and Gebremichael Y (2017b) A quantitative systems physiology model of renal function and blood pressure regulation: model description. *CPT Pharmacometrics Syst Pharmacol* **6**:383–392.
- Hallow KM, Gebremichael Y, Helmlinger G, and Vallon V (2017) Primary proximal tubule hyperreabsorption and impaired tubular transport counterregulation determine glomerular hyperfiltration in diabetes: a modeling analysis. *Am J Physiol Renal Physiol* **312**:F819–F835.
- Hallow KM, Greasley PJ, Helmlinger G, Chu L, Heerspink HJL, and Boulton DW (2018a) Evaluation of renal and cardiovascular protection mechanisms of SGLT2 inhibitors: model-based analysis of clinical data. *Am J Physiol Renal Physiol* **315**: F1295–F1306.
- Hallow KM, Helmlinger G, Greasley PJ, McMurray JJV, and Boulton DW (2018b) Why do SGLT2 inhibitors reduce heart failure hospitalization? A differential volume regulation hypothesis. *Diabetes Obes Metab* **20**:479–487.
- Hallow KM, Lo A, Beh J, Rodrigo M, Ermakov S, Friedman S, de Leon H, Sarkar A, Xiong Y, Sarangapani R, et al. (2014) A model-based approach to investigating the pathophysiological mechanisms of hypertension and response to antihypertensive therapies: extending the Guyton model. *Am J Physiol Regul Integr Comp Physiol* **306**:R647–R662.
- Hammon M, Grossmann S, Linz P, Kopp C, Dahlmann A, Garlisch C, Janka R, Cavallaro A, Luft FC, Uder M, et al. (2015) <sup>23</sup>Na magnetic resonance imaging of the lower leg of acute heart failure patients during diuretic treatment. *PLoS One* **10**:e0141336.
- Heerspink HJ, Johnsson E, Gause-Nilsson I, Cain VA, and Sjöström CD (2016) Dapagliflozin reduces albuminuria in patients with diabetes and hypertension receiving renin-angiotensin blockers. *Diabetes Obes Metab* **18**:590–597.
- Holtkamp FA, de Zeeuw D, Thomas MC, Cooper ME, de Graeff PA, Hillege HJ, Parving HH, Brenner BM, Shahinfar S, and Lambers Heerspink HJ (2011) An acute fall in estimated glomerular filtration rate during treatment with losartan predicts a slower decrease in long-term renal function. *Kidney Int* **80**: 282–287.
- Kamei S, Iwamoto M, Kameyama M, Shimoda M, Kinoshita T, Obata A, Kimura T, Hirukawa H, Tatsumi F, Kohara K, et al. (2018) Effect of tofogliflozin on body composition and glycemic control in Japanese subjects with type 2 diabetes mellitus. *J Diabetes Res* **2018**:6470137.
- Kohan DE, Fioretto P, Tang W, and List JF (2014) Long-term study of patients with type 2 diabetes and moderate renal impairment shows that dapagliflozin reduces weight and blood pressure but does not improve glycemic control. *Kidney Int* **85**: 962–971.
- Lambers Heerspink HJ, de Zeeuw D, Wie L, Leslie B, and List J (2013) Dapagliflozin a glucose-regulating drug with diuretic properties in subjects with type 2 diabetes. *Diabetes Obes Metab* **15**:853–862.
- Lazzara MJ and Deen WM (2007) Model of albumin reabsorption in the proximal tubule. *Am J Physiol Renal Physiol* **292**:F430–F439.
- Levine DZ, Iacovitti M, and Robertson SJ (2008) Modulation of single-nephron GFR in the db/db mouse model of type 2 diabetes mellitus. II. Effects of renal mass reduction. *Am J Physiol Regul Integr Comp Physiol* **294**:R1840–R1846.
- Lewis EJ, Hunsicker LG, Clarke WR, Berl T, Pohl MA, Lewis JB, Ritz E, Atkins RC, Rohde R, and Raz I; Collaborative Study Group (2001) Renoprotective effect of the angiotensin-receptor antagonist irbesartan in patients with nephropathy due to type 2 diabetes. *N Engl J Med* **345**:851–860.
- List JF, Woo V, Morales E, Tang W, and Fiedorek FT (2009) Sodium-glucose cotransport inhibition with dapagliflozin in type 2 diabetes. *Diabetes Care* **32**: 650–657.
- Mahato HS, Ahlstrom C, Jansson-Löfmark R, Johansson U, Helmlinger G, and Hallow KM (2018) Mathematical model of hemodynamic mechanisms and consequences of glomerular hypertension in diabetic mice. *NPJ Syst Biol Appl* **5**:2.
- Mann JF, Schmieder RE, McQueen M, Dyal L, Schumacher H, Pogue J, Wang X, Maggioni A, Budaj A, Chaitiraphan S, et al.; ONTARGET investigators (2008) Renal outcomes with telmisartan, ramipril, or both, in people at high vascular risk (the ONTARGET study): a multicentre, randomised, double-blind, controlled trial. *Lancet* **372**:547–553.
- Marre M, Puig JG, Kokot F, Fernandez M, Jermendy G, Opie L, Moyseev V, Scheen A, Ionescu-Tirgoviste C, Saldanha MH, et al. (2004) Equivalence of indapamide SR and enalapril on microalbuminuria reduction in hypertensive patients with type 2 diabetes: the NESTOR Study. *J Hypertens* **22**:1613–1622.
- Maruyama T, Takashima H, Oguma H, Nakamura Y, Ohno M, Utsunomiya K, Furukawa T, Tei R, and Abe M (2019) Canagliflozin improves erythropoiesis in diabetes patients with anemia of chronic kidney disease. *Diabetes Technol Ther* **21**: 713–720.
- McMurray JJV, Solomon SD, Inzucchi SE, Køber L, Kosiborod MN, Martinez FA, Ponikowski P, Sabatine MS, Anand IS, Bøhlháve J, et al.; DAPA-HF Trial Committees and Investigators (2019) Dapagliflozin in patients with heart failure and reduced ejection fraction. *N Engl J Med* **381**:1995–2008.
- Mikami Y, Takagi K, Itaya Y, Ono Y, Matsumura H, Takai Y, and Seki H (2014) Postpartum recovery course in patients with gestational hypertension and pre-eclampsia. *J Obstet Gynaecol Res* **40**:919–925.
- Mosenzon O, Wiviott SD, Cahn A, Rozenberg A, Yanuv I, Goodrich EL, Murphy SA, Heerspink HJL, Zelniker TA, Dwyer JP, et al. (2019) Effects of dapagliflozin on development and progression of kidney disease in patients with type 2 diabetes: an analysis from the DECLARE-TIMI 58 randomised trial. *Lancet Diabetes Endocrinol* **7**:606–617.
- Ohara K, Masuda T, Murakami T, Imai T, Yoshizawa H, Nakagawa S, Okada M, Miki A, Myoga A, Sugase T, et al. (2019) Effects of the sodium-glucose cotransporter 2 inhibitor dapagliflozin on fluid distribution: a comparison study with furosemide and tolvaptan. *Nephrology (Carlton)* **24**:904–911.

- Parving HH, Persson F, Lewis JB, Lewis EJ, and Hollenberg NK; AVOID Study Investigators (2008) Aliskiren combined with losartan in type 2 diabetes and nephropathy. *N Engl J Med* **358**:2433–2446.
- Pessoa TD, Campos LC, Carraro-Lacroix L, Girardi AC, and Malnic G (2014) Functional role of glucose metabolism, osmotic stress, and sodium-glucose cotransporter isoform-mediated transport on Na<sup>+</sup>/H<sup>+</sup> exchanger isoform 3 activity in the renal proximal tubule. *J Am Soc Nephrol* **25**:2028–2039.
- Petrykiv S, Sjöström CD, Greasley PJ, Xu J, Persson F, and Heerspink HJL (2017) Differential effects of dapagliflozin on cardiovascular risk factors at varying degrees of renal function. *Clin J Am Soc Nephrol* **12**:751–759.
- Titze J (2009) Water-free sodium accumulation. *Semin Dial* **22**:253–255.
- Titze J (2014) Sodium balance is not just a renal affair. *Curr Opin Nephrol Hypertens* **23**:101–105.
- Vallon V and Thomson SC (2017) Targeting renal glucose reabsorption to treat hyperglycaemia: the pleiotropic effects of SGLT2 inhibition. *Diabetologia* **60**: 215–225.
- van Bommel EJM, Muskiet MHA, van Baar MJB, Tonneijck L, Smits MM, Emanuel AL, Bozovic A, Danser AHJ, Geurts F, Hoorn EJ, et al. (2020) The renal hemodynamic effects of the SGLT2 inhibitor dapagliflozin are caused by post-glomerular vasodilatation rather than pre-glomerular vasoconstriction in metformin-treated patients with type 2 diabetes in the randomized, double-blind RED trial [published correction appears in *Kidney Int* (2020) 97:1061]. *Kidney Int* **97**:202–212.
- Wada Y, Hamamoto Y, Nakatani Y, Fujikawa J, Iwasaki Y, Yoshiji S, Aizawa-Abe M, Iwasaki K, Honjo S, and Hamasaki A (2019) 2343-PUB: reduction of HbA1c after SGLT2 inhibitors correlate with change in plasma osmolarity but not with elevation of hematocrit in Japanese patients with type 2 diabetes. *Diabetes* **68**.
- Wang W, Hallow KM, and James DA (2016) A tutorial on RxODE: simulating differential equation pharmacometric models in R. *CPT Pharmacometrics Syst Pharmacol* **5**:3–10.
- Wanner C, Inzucchi SE, Lachin JM, Fitchett D, von Eynatten M, Mattheus M, Johansen OE, Woerle HJ, Broedl UC, and Zinman B; EMPA-REG OUTCOME Investigators (2016) Empagliflozin and progression of kidney disease in type 2 diabetes. *N Engl J Med* **375**:323–334.
- Wilding JP, Norwood P, Tjoen C, Bastien A, List JF, and Fiedorek FT (2009) A study of dapagliflozin in patients with type 2 diabetes receiving high doses of insulin plus insulin sensitizers: applicability of a novel insulin-independent treatment. *Diabetes Care* **32**:1656–1662.
- Yamout H, Perkovic V, Davies M, Woo V, de Zeeuw D, Mayer C, Vijapurkar U, Kline I, Usiskin K, Meininger G, et al. (2014) Efficacy and safety of canagliflozin in patients with type 2 diabetes and stage 3 nephropathy. *Am J Nephrol* **40**:64–74.
- Yavin Y, Mansfield TA, Ptaszynska A, Johnsson K, Parikh S, and Johnsson E (2016) Effect of the SGLT2 inhibitor dapagliflozin on potassium levels in patients with type 2 diabetes mellitus: a pooled analysis. *Diabetes Ther* **7**:125–137.
- Zinman B, Wanner C, Lachin JM, Fitchett D, Bluhmki E, Hantel S, Mattheus M, Devins T, Johansen OE, Woerle HJ, et al.; EMPA-REG OUTCOME Investigators (2015) Empagliflozin, cardiovascular outcomes, and mortality in type 2 diabetes. *N Engl J Med* **373**:2117–2128.

---

**Address correspondence to:** K. Melissa Hallow, Department of Chemical, Materials, and Biomedical Engineering, University of Georgia, 597 D.W. Brooks Dr., Athens, GA 30602. E-mail: Hallowkm@uga.edu

---

## Supplemental Material

**Manuscript Title:** Renal effects of dapagliflozin in people with and without diabetes with moderate or severe renal dysfunction: prospective modeling of an ongoing clinical trial.

K. Melissa Hallow<sup>1</sup>, David W. Boulton<sup>2a</sup>, Robert C. Penland<sup>2b</sup>, Gabriel Helmlinger<sup>2b</sup>, Emily Nieves<sup>1</sup>, Daniël H. van Raalte<sup>3</sup>, Hiddo L Heerspink<sup>4,5</sup>, Peter J. Greasley<sup>6</sup>

1. Department of Chemical, Materials, and Biomedical Engineering, University of Georgia, Athens, GA, USA

2. Clinical Pharmacology and Quantitative Pharmacology, Clinical Pharmacology and Safety Sciences, R&D, AstraZeneca, <sup>a</sup>Gaithersburg, MD, USA, <sup>b</sup>Waltham, MA, USA, <sup>c</sup>Gothenburg, Sweden

3. Diabetes Center, Department of Internal Medicine, Amsterdam University Medical Centers, location VUMC, Amsterdam, The Netherlands

4. Department of Clinical Pharmacy and Pharmacology, University of Groningen, Groningen, Netherlands

5. The George Institute for Global Health, Sydney, Australia

6. Early Clinical Development, Research and Early Development, Cardiovascular, Renal and Metabolism (CVRM) BioPharmaceuticals R&D, AstraZeneca, Gothenburg, Sweden and AstraZeneca R&D, Gothenburg, SE-431 83

Journal of Experimental Pharmacology and Therapeutics

JPET-AR-2020-000040

### FULL MODEL EQUATIONS

#### Renal Vasculature

The glomeruli are modeled in parallel, and in series with the preafferent (interlobar, interlobular, and arcuate arterioles) and peritubular vasculature. Glomerular capillary resistance is assumed negligible. Thus, renal vascular resistance RVR is given by:

$$RVR = R_{preaff} + \frac{(R_{aa} + R_{ea})}{N_{nephrons}} + R_{peritubular} \quad \text{Eq. A1}$$

$R_{preaff}$  and  $R_{peritubular}$  are lumped resistances describing the total resistance of preafferent and peritubular vasculatures, respectively, while  $R_{aa}$  and  $R_{ea}$  are the resistances of a single afferent or efferent arteriole, as determined from Pouissele's law, based on the arteriole's diameter  $d$ , length  $L$ , and blood viscosity  $\mu$ :

$$R_{aa} = \frac{128\mu L_{aa}}{\pi d_{aa}^4}; \quad R_{ea} = \frac{128\mu L_{ea}}{\pi d_{ea}^4} \quad \text{Eq. A2}$$

$N_{nephrons}$  is the number of nephrons. All nephrons are assumed identical, and the model does not account for spatial heterogeneity.

Renal blood flow (RBF) is a function of the pressure drop across the kidney and RVR, according to Ohm's law:

$$RBF = \frac{MAP - P_{renal-vein}}{RVR} + \frac{GFR \left( \frac{R_{ea}}{N_{nephrons}} \right)}{RVR} \quad \text{Eq. A3}$$

Renal venous pressure ( $P_{renal-vein}$ ) is treated as constant. The second term in this equation accounts for lower flow through the efferent arterioles due to GFR. As an approximation, all filtrate is assumed reabsorbed back into the peritubular capillaries, so that peritubular flow is the same as afferent flow.

$P_{gc}$  is determined according to Ohm's law:

$$P_{gc} = MAP - RBF * (R_{preaff} + R_{aa}/N_{nephrons}) \quad \text{Eq. A4}$$

Determination of MAP,  $P_{Bow}$  and  $\pi_{go-avg}$  are described later.

Single nephron glomerular filtration rate (SNGFR) is defined according to Starling's equation, where  $K_f$  is the glomerular ultrafiltration coefficient,  $P_{gc}$  is glomerular capillary hydrostatic pressure,  $P_{Bow}$  is pressure in the Bowman's space, and  $\pi_{go-avg}$  is average glomerular capillary oncotic pressure.

$$SNGFR = K_f (P_{gc} - P_{Bow} - \pi_{go-avg}) \quad \text{Eq. A5}$$

The total GFR is then the SNGFR multiplied by the number of nephrons:

$$GFR = SNGFR * N_{nephrons} \quad \text{Eq. A6}$$

### Glucose filtration, reabsorption, and excretion

Glucose is filtered freely through the glomerulus, so that single nephron filtered glucose load is:

$$\Phi_{glu,filtered} = SNGFR * C_{glu} \quad \text{Eq. A7}$$

where  $C_{glu}$  is the plasma glucose concentration.

Glucose reabsorbed in the S1 and S2 segments is given by:

$$\Phi_{glu,reabs,S12} = \min(\Phi_{glu,filtered}, J_{glu,S12} * L_{pt,S12}) \quad \text{Eq. A8}$$

where  $J_{glu,S12}$  is the rate of glucose reabsorption per unit length of the S1 and S2 segments together, and  $L_{pt,S12}$  is the length of the PT S1 and S2 segments together. Similarly, glucose reabsorbed in the S3 segment is given by:

$$\Phi_{glu,reabs,S3} = \min(J_{glu,S3} * L_{pt,S3}, \Phi_{glu,filtered} - \Phi_{glu,reabs,S12}) \quad \text{Eq. A9}$$

Any unreabsorbed glucose then flows through the rest of the tubule and is ultimately excreted, so that the rate of urinary glucose excretion ( $R_{UGE}$ ) is:

$$R_{UGE} = \Phi_{glu,out-PT} = \Phi_{glu,filtered} - \Phi_{glu,reabs,S12} - \Phi_{glu,reabs,S3} \quad \text{Eq. A10}$$

Glucose reabsorption occurs exclusively in the PT through  $\text{Na}^+$  glucose cotransporters (SGLT). SGLT2 in the S1 and S2 segments of the PT reabsorbs 90-97% of filtered glucose, while SGLT1 in the S3 segment reabsorbs the remaining 3-10%(39-43). At high plasma glucose concentrations, filtered glucose can exceed the kidney's capacity for reabsorption, and the excess glucose is excreted.  $J_{glu,S12}$  and  $J_{glu,S3}$  represent the number and function of SGLT2 and SGLT1 transporters respectively. The values were determined such that 95% of filtered glucose is reabsorbed in the S1 and S2 segments, while the remaining glucose was reabsorbed in the S3 segment, and so that all glucose is reabsorbed and urinary glucose excretion is zero for blood glucose concentrations up to 9 mmol/l(44).

### **$\text{Na}^+$ filtration and reabsorption in the PT**

Similarly to glucose,  $\text{Na}^+$  is freely filtered across the glomerulus, so that the single nephron filtered  $\text{Na}^+$  load is given by:

$$\Phi_{\text{Na},filtered} = SNGFR * C_{\text{Na}} \quad \text{Eq.A11}$$



where  $C_{Na}$  is the plasma  $Na^+$  concentration.

The rate of  $Na^+$  reabsorption through SGLT2 equals the rate of glucose reabsorption in the S1 and S2 segments, since SGLT2 reabsorb sodium and glucose at a 1:1 molar ratio:

$$\Phi_{Na, reabs-SGLT2} = \Phi_{glu, reabs, S12} \quad \text{Eq. A12}$$

The rate of  $Na^+$  reabsorption through SGLT1 is twice the rate of glucose reabsorption in the S3 segment, since SGLT1 reabsorb sodium and glucose at a 2:1 molar ratio:

$$\Phi_{Na, reabs-SGLT1} = 2 * \Phi_{glu, reabs, S3} \quad \text{Eq. A13}$$

Total PT  $Na^+$  reabsorption is then given by:

$$\Phi_{Na, reabs-PT} = \Phi_{Na, filtered} * (\eta_{Na, reabs-PT, NHE3} + \eta_{Na, reabs-PT, other}) + \Phi_{Na, reabs-SGLT2} + \Phi_{Na, reabs-SGLT1} \quad \text{Eq. A14}$$

where  $\eta_{Na, reabs-PT, NHE3}$  and  $\eta_{Na, reabs-PT, other}$  are the fractional rates of PT sodium reabsorption through NHE3, and through mechanisms other than SGLT2 and NHE3.  $Na^+$  flow rate out of the PT is then:

$$\Phi_{Na, out-PT} = \Phi_{Na, filtered} - \Phi_{Na, reabs-PT} \quad \text{Eq. A15}$$

For the remaining nephron segments, we approximate Na reabsorption in each segment as distributed uniformly along the length, and the rate of reabsorption per unit length is formulated so that the degree of flow-dependence can be varied. For a given segment, the nominal rate of reabsorption per unit length  $r_{i,0}$  is given by the following, where  $\eta$  is the baseline fractional rate of reabsorption,  $\Phi_{Na,0}(0)$  is the rate delivered to the segment under baseline conditions, and  $L$  is the segment length.

$$r_{i,0} = \frac{\eta_i \Phi_{Na,i0}(0)}{L_i} \quad \text{Eq. A16}$$

where i is the ascending LoH (ALH), DCT, or CNT/CD.

The actual rate per unit length  $r_i$  is then the nominal rate augmented by a flow-dependent component, as shown in Eq 17. The coefficient B determines the degree of flow-dependence: for B=0, there is no flow dependence; for B=1, changes in reabsorption are directly proportional to flow.

$$r_i = r_{i,0} + \frac{B_i \eta_i (\Phi_{Na,i}(0) - \Phi_{Na,i0}(0))}{L_i} \quad \text{Eq. A17}$$

Na flow along each segment is then:

$$\Phi_{Na,i}(x) = \Phi_{Na,i}(0) - r_i x \quad \text{Eq. A18}$$

$\Phi_{Na,i}(0)$  is obtained from the Na flow out of the preceding tubule segment.

### Water Reabsorption along the tubule

Water reabsorption in the PT is isosmotic. Therefore, water leaving the PT and entering the loop of Henle is given by:

$$\Phi_{water,out-PT} = \Phi_{water,in-DCT} = SNGFR * \frac{\Phi_{osm,filtered}}{\Phi_{osm,out-PT}} \quad \text{Eq. A19}$$

where filtered osmolytes include both sodium and glucose:

$$\Phi_{osm,filtered} = 2 * \Phi_{Na,filtered} + \Phi_{glu,filtered} \quad \text{Eq. A20}$$

$$\Phi_{osm,out-PT} = 2 * \Phi_{Na,out-PT} + \Phi_{glu,out-PT} \quad \text{Eq. A21}$$

In the loop of Henle (LoH), water is reabsorbed in the water permeable descending LoH (DLH) due to the osmotic gradient created by actively pumping sodium out of the water-impermeable ascending limb (ALH). The osmolality along the length of the DLH  $Osm_{DLH}$ , which is assumed in equilibrium with the osmolality in the surrounding interstitium  $Osm_{IS}$ , is given by:

$$Osm_{DLH}(x) = Osm_{IS}(x) = Osm_{DLH}(0)e^{\frac{r_{ALH}x}{\Phi_{water,in-DCT}Osm_{DLH}(0)}} \quad \text{Eq. A22}$$

Here,  $x$  is the distance along the tubule length, and  $R_{ALH}$  is the rate of sodium reabsorption per unit length in the ascending loop of Henle (Eq. A17). Water flow through the DLH is then given by:

$$\Phi_{water,DLH}(x) = \frac{\Phi_{water,DLH}(0)Osm_{DLH}(0)}{Osm_{DLH}(x)} \quad \text{Eq. A23}$$

The ALH and the distal convoluted tubule (DCT) are modeled as impermeable to water, so that the flow through these segments equals the flow out of the DLH:

$$\Phi_{water,ALH}(x) = \Phi_{water,DCT}(x) = \Phi_{water,DLH}(L) \quad \text{Eq. A24}$$

In the collecting duct (CD), water reabsorption is driven by the osmotic gradient between the CD tubular fluid and the interstitium, and is modulated by vasopressin, as described later:

$$\Phi_{water,reabs-CD} = \mu_{vasopressin} \Phi_{water,CD}(0) * \left(1 - \frac{Osm_{CD}(L)}{Osm_{IS}(L)}\right) \quad \text{Eq. A25}$$

Where the osmolality in the CD  $Osm_{CD}(L)$  accounts for sodium reabsorbed in the collecting duct:

$$Osm_{CD}(L) = \frac{\Phi_{osm,cd}(0) - 2 * (\Phi_{Na,cd}(0) - \Phi_{Na,cd}(L))}{\Phi_{water,CD}(0)} \quad \text{Eq. A26}$$

Then, single nephron water excretion rate is given by:

$$\Phi_{\text{water,CD}}(L) = \Phi_{\text{water,CD}}(0) - \Phi_{\text{water, reabs-CD}} \quad \text{Eq. A27}$$

And urine flow rate is then:

$$\Phi_{\text{urine}} = \text{SNGFR} * \Phi_{\text{water,CD}}(L) \quad \text{Eq. A28}$$

### Whole Body Sodium and Water Balance and Peripheral Sodium Storage

We incorporated that three compartment model of volume homeostasis into the renal physiology model, to allow evaluation of the potential role of peripheral sodium storage in the renal response to dapagliflozin. Titze et al have demonstrated dynamic changes in non-osmotically stored sodium in peripheral tissues (Hammon et al. 2015), and we have previously shown that this mechanism is necessary in order explain constant plasma Na<sup>+</sup> concentration observed with electrolyte-free water clearance with SGLT2 inhibition (Hallow et al., 2017). Parameters for this portion of the model are given in Table S1. Sodium and water are assumed to move freely between the blood and interstitial fluid. Water and sodium intake rates were assumed constant. Then blood volume ( $V_b$ ) and blood sodium ( $\text{Na}_{\text{blood}}$ ) are the balance between intake and excretion of water and sodium respectively, and the intercompartmental transfer.

$$\frac{d}{dt}(V_b) = \text{Water}_{\text{in}} - \text{Water}_{\text{out}} + Q_{\text{water}}([\text{Na}]_{\text{blood}} - [\text{Na}]_{\text{IF}}) \quad \text{Eq. A29}$$

$$\frac{d}{dt}(\text{Na}_{\text{blood}}) = \Phi_{\text{Na,intake}} - \Phi_{\text{Na,excretion}} + Q_{\text{Na}}([\text{Na}]_{\text{IF}} - [\text{Na}]_{\text{blood}}) \quad \text{Eq. A30}$$

Sodium concentrations in the blood and interstitial compartments are assumed to equilibrate quickly. Change in interstitial fluid volume (IFV) is a function of intercompartmental water transfer.

$$\frac{d}{dt}(\text{IFV}) = Q_{\text{water}}([\text{Na}]_{\text{IF}} - [\text{Na}]_{\text{blood}}) \quad \text{Eq. A31}$$

When interstitial sodium concentration  $[Na]_{IF}$  exceeds the normal equilibrium level  $[Na]_{IF,ref}$ ,  $Na^+$  moves out of the interstitium and is sequestered in the peripheral  $Na^+$  compartment, at a rate of  $\Phi_{Na,stored}$ , where it is osmotically inactive. Thus, the change interstitial fluid sodium depends on intercompartmental transfer and peripheral storage. Sodium cannot be stored indefinitely, and thus there is a limit  $N_{a,stored,max}$  on how much sodium can be stored. The peripheral sodium compartment can be effectively removed from the model by setting  $Q_{Na,stored}$  to zero.

$$\Phi_{Na,stored} = Q_{Na,stored} * \frac{(N_{a,stored,max} - N_{a,stored})}{N_{a,stored,max}} ([Na]_{JF} - [Na]_{IF,ref}) \quad \text{Eq. A32}$$

$$\frac{d}{dt}(N_{a,stored}) = \Phi_{Na,stored} \quad \text{Eq. A33}$$

$$\frac{d}{dt}(Na_{IF}) = Q_{Na}([Na]_{blood} - [Na]_{IF}) - \Phi_{Na,stored} \quad \text{Eq. A34}$$

Blood and IF sodium concentrations are then given by:

$$[Na]_{blood} = \frac{Na_{blood}}{V_B} \quad \text{Eq. A35}$$

$$[Na]_{IF} = \frac{Na_{IF}}{IFV} \quad \text{Eq. A36}$$

### **Tubular Hydrostatic Pressure**

Hydrostatic pressure in the Bowman's space is a key factor affecting GFR, and this pressure is influenced by both morphology and flow rates through the tubule. Changes in  $Na$  and water reabsorption along the nephron, which can occur either due to disease or treatments, can alter GFR by altering tubular pressures. Thus dynamically modeling tubular pressures can be critical to understanding GFR changes.

Adapting from Jensen et al(16), tubular flow rates described in the main text can be used to determine tubular pressure. The change in intratubular pressure  $dP^*$  over a length of tubule  $dx$  can be defined according to Poiseuille's law as:

$$dP^* = -\frac{128\mu}{\pi D^4} \Phi_{\text{water}}(x) dx \quad \text{Eq. A37}$$

Eq. 36 describes the relationship between transtubular pressure  $P$  and tubular diameter  $D$ , where  $D_c$  is the diameter at control pressure  $P_c$ , and  $\beta$  is the exponent of tubular distensibility.

$$\frac{D}{D_c} = \left(\frac{P}{P_c}\right)^\beta \quad \text{Eq. A38}$$

Substituting and assuming uniform interstitial pressure throughout the kidney, we obtain:

$$dP = -\frac{128\eta}{\pi D_c^4} \left(\frac{P_c}{P}\right)^{4\beta} \Phi_{\text{water}}(x) dx \quad \text{Eq A39}$$

Integrating over a tubule segment length, we obtain inlet pressure as a function of the outlet pressure and the flow rate:

$$P_{\text{in}} = \left[ P_{\text{out}}^{4\beta+1} + \frac{(4\beta+1)128\eta P_c^{4\beta}}{\pi D_c^4} \int_0^L \Phi_{\text{water}}(x) dx \right]^{\frac{1}{4\beta+1}} \quad \text{Eq A40}$$

The pressure calculated at the inlet to the PT is used as  $P_{\text{Bow}}$  in Eq. A5 above.

Because the diameter of the CNT/CD changes as nephrons coalesce, calculating pressure along this segment is challenging. Under normal conditions, pressure drops 5-7mmHg across the CNT/CD. Thus, an effective control diameter was calculated to give this degree of pressure drop under baseline conditions.

### **Glomerular Capillary Oncotic Pressure**

The glomerular capillary oncotic pressure is calculated using the Landis Pappenheimer equation, where  $C_{\text{prot}}$  is the concentration of protein at the point of interest.



$$\pi = 1.629 * C_{\text{prot}} + 0.2935 * C_{\text{prot}}^2 \quad \text{Eq. A41}$$

Plasma protein ( $C_{\text{prot-plasma}}$ ) is assumed constant. Protein concentration at the distal end of the glomerulus ( $C_{\text{prot-glom-out}}$ ) is determined as:

$$C_{\text{prot-glom-out}} = C_{\text{prot-plasma}} * \frac{\text{RBF}}{\text{RBF} - \text{GFR}} \quad \text{Eq. A42}$$

Protein concentration is assumed to be varying linearly along the capillary length, and thus the oncotic pressure  $\pi_{go-avg}$  is calculated using the average of the plasma protein concentration and protein concentration at the distal end of the glomerulus.

The model does not account for filtration equilibrium, which may occur in some species.

## Regulatory Mechanisms

Multiple control mechanisms act on the system to allow simultaneous control of  $C_{\text{na}}$ , CO, MAP, glomerular pressure, and RBF. For each control mechanism, the feedback signal  $\mu$  is modeled by one of two functional forms. The choice of functional form is determined by whether a steady state error is allowed in the controlled variable  $X$ . When a steady state error is not allowed (i.e.  $X$  always eventually returns to the setpoint  $X_0$ ), the effect is defined by a proportional-integral (PI) controller. The initial feedback signal is proportional to the magnitude of the error ( $X - X_0$ ), with gain  $G$ . But the feedback continues to grow over time as long as any error exists, until the error returns to zero. The integral gain  $K_i$  determines the speed of return to steady-state.

$$\mu = 1 + G * ((X - X_0) + K_i * \int (X - X_0) dt) \quad \text{Eq. A43}$$

All other mechanisms, for which the controlled variable can deviate from the setpoint at steady-state, are described by a logistic equation that produces a saturating response characteristic of biological signals:

$$\mu = 1 + S * \left( \frac{1}{1 + \exp\left(\frac{X - X_0}{m}\right)} - 0.5 \right) \quad \text{Eq. A44}$$

Here,  $m$  defines the slope of the response around the operating point, and  $S$  is the maximal response as  $X$  goes to  $\pm\infty$ .

### **Control of plasma Na concentration by vasopressin**

Changes in plasma osmolality are sensed via osmoreceptors, stimulating vasopressin secretion, which exerts control of water reabsorption in the CNT/CD. To insure that blood sodium concentration  $C_{Na}$  is maintained at its setpoint  $C_{Na,0}$  at steady state, this process is modeled by a PI controller:

$$\mu_{\text{vasopressin}} = 1 + G_{Na-vp} * (C_{Na} + K_{i-vp} * \int (C_{Na} - C_{Na,0}) dt) \quad \text{Eq. A45}$$

The parameters  $G_{Na-vp}$  and  $K_{i-vp}$  are gains of proportional and integral control, respectively.

### **Tubular Pressure Natriuresis**

For homeostasis, Na excretion over the long-term must exactly match Na intake (the principle of Na balance). Any steady-state Na imbalance would lead to continuous volume retention or loss— an untenable situation. Pressure-natriuresis(2), wherein changes in renal perfusion pressure (RPP) induce changes in Na excretion, insures that Na balance is maintained. It may be partially achieved through neurohumoral mechanisms including the RAAS, but there is also an intrinsic pressure-mediated effect on tubular Na reabsorption, where renal interstitial hydrostatic pressure (RIHP) is believed to be the driving signal. RIHP is a function of peritubular capillary pressure, and is calculated according to Ohm's law:

$$P_{\text{peritubular}} = \text{MAP} - \text{RBF} * \left( R_{\text{preaff}} + \frac{R_{\text{aff}} + R_{\text{eff}}}{N_{\text{nephrons}}} \right) \quad \text{Eq. A46}$$

As a simplification, we assume an increase in peritubular pressure will generate a proportional increase in RIHP. Since the kidney is encapsulated, we assume interstitial pressure equilibrates and changes in one

region are transduced across the kidney. The relationship between RIHP and fractional Na reabsorption rate of each tubular segment is then modeled as:

$$\eta_{i-sodreab} = \eta_{i-sodreab,0} * \left( 1 + S_{P-N,i} * \left( \frac{1}{1+\exp(RIHP - RIHP_0)} - 0.5 \right) \right) \quad \text{Eq. A47}$$

where  $i = \text{PT, LoH, DCT, or CNT/CD}$ .  $\eta_{i-sodreab,0}$  is the nominal fractional rate of reabsorption for that tubule segment.  $RIHP_0$  defines the setpoint pressure and is determined from RIHP at baseline for normal Na intake.  $S_{P-N,i}$  defines the maximal signal as RIHP goes to  $\infty$ .

### Control of Cardiac Output

CO, which describes total blood flow to body tissues, returns to normal over days to weeks following a perturbation (38). CO regulation is a complex phenomenon that occurs over multiple time scales, but we focus only on long-term control (days to weeks), which is thought to be achieved through whole-body autoregulation - the intrinsic ability of organs to adjust their resistance to maintain constant flow(38). The total effect of local autoregulation of all organs is that TPR is adjusted to maintain CO at a constant resting level. The feedback between CO and TPR is modeled with a PI controller, such that CO is controlled to its steady-state setpoint  $CO_0$ .

$$TPR = TPR_0 * \left( 1 + G_{CO-tpR} * (CO + K_{i-tpR} * \int (CO - CO_0) dt) \right) \quad \text{Eq. A48}$$

### Control of Macula Densa Sodium Concentration by Tubuloglomerular Feedback

Tubuloglomerular feedback (TGF) helps stabilize tubular flow by sensing Na concentration in the the macula densa, which sits between the LoH and DCT, and providing a feedback signal to inversely change afferent arteriole diameter. The TGF effect is defined as:

$$\mu_{\text{TGF}} = 1 + S_{\text{TGF}} * \left( \frac{1}{1 + \exp\left(\frac{C_{\text{Na,MD},0} - C_{\text{Na,MD}}}{m_{\text{TGF}}}\right)} - 0.5 \right) \quad \text{Eq. A49}$$

The basal afferent arteriole resistance  $R_{\text{aa}}$  is then multiplied by  $\mu_{\text{TGF}}$  to obtain the ambient afferent arteriolar resistance. The setpoint  $C_{\text{Na,MD},0}$  is the Na concentration out of the LoH and into the DCT in the baseline state at normal Na intake.

### Myogenic Autoregulation of Glomerular Pressure

Glomerular hydrostatic pressure is normally tightly autoregulated, and changes very little in response to large changes in blood pressure. This autoregulation is in part through myogenic autoregulation of the preglomerular arterioles. While the pressure drop and thus myogenic response varies along the arteriole length, we make the simplifying assumption that the preafferent vasculature responds to control pressure at the distal end.

$$\mu_{\text{autoreg}} = 1 + S_{\text{autoreg}} * \left( \frac{1}{1 + \exp\left(\frac{P_{\text{preafferent}} - P_{\text{preafferent},0}}{m_{\text{autoreg}}}\right)} - 0.5 \right) \quad \text{Eq. A50}$$

Pressure at the distal end of the preafferent vasculature is given by:

$$P_{\text{preafferent}} = \text{MAP} - \text{RBF} * R_{\text{preaff}} \quad \text{Eq. A51}$$

The basal preafferent arteriole resistance  $R_{\text{preaff}}$  is then multiplied by  $\mu_{\text{autoreg}}$  to obtain the ambient preafferent arteriolar resistance.

### Renin-Angiotensin-Aldosterone System Submodel

Renin is secreted at a nominal rate  $\text{SEC}_{\text{ren},0}$  modulated by macula densa sodium flow, as well as by a strong negative feedback from Angiotensin II bound to the AT1 receptor.

$$SEC_{renin} = \mu_{md-renin} * \mu_{AT1} * \mu_{rsna} * SEC_{renin,0} \quad \text{Eq. A52}$$

The macula densa releases renin in response to reduced sodium flow:

$$\mu_{md-renin} = e^{-A_{md-ren}(\phi_{Na,md} - \phi_{Na,md,0})} \quad \text{Eq. A53}$$

We have found that the inhibitory effect of AT1-bound AngII on renin secretion can be well described by the following relationship:

$$\mu_{AT1} = A_{AT1,ren} \left( \frac{AT1-bound-AngII}{AT1-bound-AngII_0} \right) \quad \text{Eq. A54}$$

Renal sympathetic nerve activity is assumed to exert a linear effect on renin secretion. Renin secretion may also be controlled by baroreceptors in the afferent arteriole. However, it is difficult to distinguish between the effects of macula densa sodium flow and preafferent pressure in most experiments, since these variables move in the same direction. As a simplifying assumption, and because we have previously found that it provides a better fit to available data (results not published), we neglected the baroreceptor effect and implicitly assume that it is accounted for by the effect of macula-densa sodium flow.

Plasma renin concentration (PRC) is then given by:

$$\frac{d(PRC)}{dt} = SEC_{renin} - K_{d,renin} * PRC \quad \text{Eq. A55}$$

Where  $K_{d,renin}$  is the renin degradation rate. PRA can be related to PRC by the conversion factor 0.06 (ng/ml/hr)/(pg/ml).

Angiotensin I is formed by PRA, assuming that its precursor angiotensinogen is available in excess and the plasma renin activity (PRA) is the rate-limiting step. AngI is also converted to AngII by the enzymes ACE and chymase, and is degraded at a rate of  $K_{d,AngI}$ .

$$\frac{d(AngI)}{dt} = PRA - (ACE + Chymase) * AngI - K_{d,AngI} AngI \quad \text{Eq. A56}$$

Angiotensin II is formed from the action of ACE and chymase on AngI, can be eliminated by binding to either the AT1 or AT2 receptors at the rate  $K_{AT1}$  and  $K_{AT2}$  respective, and is degraded at a rate of  $K_{d,AngII}$ .

$$\frac{d(AngII)}{dt} = (ACE + Chymase) * AngI - (K_{AT1} + K_{AT2}) * AngII - K_{d,AngII} AngII \quad \text{Eq. A57}$$

The complex of Angiotensin II bound to the AT1 receptor is the physiologically active entity within the pathway, and is given by:

$$\frac{d(AT1_{bound} AngII)}{dt} = (K_{AT1}) * AngII - K_{d,AT1} AT1_{bound} AngII \quad \text{Eq. A58}$$

AT1-bound AngII has multiple physiologic effects, including constriction of the efferent, as well and preglomerular, afferent, and systemic vasculature, sodium retention in the PT, and aldosterone secretion.

Each effect is modeled as:

$$\mu_{AT1,i} = 1 + S_{AT1,i} * \left( \frac{1}{1 + \exp\left(\frac{AT1-bound AngII_0 - AT1-bound AngII}{m_{AT1,i}}\right)} - 0.5 \right) \quad \text{Eq. A59}$$

where i represents the effect on efferent, afferent, preafferent, or systemic resistance, PT sodium reabsorption, or aldosterone secretion.

Aldosterone is the second physiologically active entity in the RAAS pathway, acting by binding to mineralocorticoid receptors (MR) in the CNT/CD and DCT to stimulate sodium reabsorption. MR-bound aldosterone is modeled as the nominal concentration Aldo<sub>0</sub> modulated by the effect of AT1-bound AngII, and the normalized availability of MR receptors (1 in the absence of an MR antagonist).

$$MR-bound\_Aldo = Aldo_0 * \mu_{AT1} * MR \quad \text{Eq. A60}$$

The effects of MR-bound aldosterone on CNT/CD and DCT sodium reabsorption are modeled as:

$$\mu_{aldo,i} = 1 + S_{aldo,i} * \left( \frac{1}{1 + \exp\left(\frac{MR-bound Aldo_0 - MR-bound Aldo}{m_{aldo,i}}\right)} - 0.5 \right) \quad \text{Eq. A61}$$

Where i is the CNT/CD or DCT.

## Cardiac Model

The ventricular mechanics portion of the model was adapted from a previously published model by Arts, Bovendeerd, and colleagues (1, 6). Many equations were used verbatim from these previous papers. We repeat those equations here for the reader's convenience, but refer the reader to the original publication for more complete explanation. Here we present equations for the left ventricle; analogous equations were used for the right ventricle.

The volume of blood inside the left ventricle chamber  $V_{lv}$  is given by:

$$\frac{d(V_{lv})}{dt} = Q_{mitral} - Q_{aorta} \quad \text{Eq. A62}$$

where  $Q_{mitral}$  and  $Q_{aorta}$  are blood flow rates through the mitral and aortic valves, respectively, as described later. Bovendeerd et al showed that left ventricular pressure  $P_{lv}$  can be related to LV volume  $V_{lv}$  and LV wall volume  $V_w$  by the following (Ref 6, Eq. 7):

$$P_{lv} = \frac{1}{3} (\sigma_f - 2\sigma_{m,r}) \ln \left( 1 + \frac{V_w}{V_{lv}} \right) \quad \text{Eq. A63}$$

Here  $\sigma_f$  and  $\sigma_{m,r}$  are mechanical stresses in the myocardium along the longitudinal fiber the radial direction respectively.  $\sigma_f$  is comprised of the sum of the passive stress along the fiber  $\sigma_{m,f}$  and active fiber stress  $\sigma_a$ . The passive stress along the fiber is a function of the longitudinal stretch along the fiber  $\lambda_f$  and the myocardial longitudinal stiffness  $c_f$  (Ref 6, Eq. 14).

$$\sigma_{m,f}(\lambda_f) = \begin{cases} \sigma_{f0} (e^{c_f(\lambda_f-1)} - 1) & \lambda_f \geq 1 \\ 0 & \lambda_f < 1 \end{cases} \quad \text{Eq. A64}$$

And mean passive radial stress is a function of the radial stretch  $\lambda_r$  and the myocardial radial stiffness  $c_r$  (Ref 6, Eq. 15).

$$\sigma_{m,r}(\lambda_r) = \begin{cases} \sigma_{r0}(e^{c_r(\lambda_r-1)} - 1) & \lambda_r \geq 1 \\ 0 & \lambda_r < 1 \end{cases} \quad \text{Eq. A65}$$

As shown by Bovendeerd et al, the longitudinal stretch  $\lambda_f$  is related to chamber blood volume and wall volume by (Ref 6, Eq. 8):

$$\lambda_f = \left( \frac{V_{lv} + \frac{1}{3}V_w}{V_{lv,cavity} + \frac{1}{3}V_w} \right)^{\frac{1}{3}} \quad \text{Eq. A66}$$

$V_{lv,cavity}$  is the chamber volume at zero transmural pressure.

The radial stretch  $\lambda_r$  is given by (Ref 6, Eq. 9):

$$\lambda_r = \lambda_f^{-2} \quad \text{Eq. A67}$$

where  $C_f$  and  $C_r$  are the stiffness of the myocardial tissue in the longitudinal and radial directions, respectively.

LV active stress is a function of contractility ( $c$ ), sarcomere length  $l_s$ , sarcomere shortening velocity  $V_s$ , and time elapsed since beginning of contraction ( $t_o$ ). These equations were taken exactly as shown in Ref 6, Eq. 10 - 13.

**Table S1. Baseline Renal Model Parameters**

Parameter	Definition	Value	Units
-----------	------------	-------	-------



$\beta$	Tubular compliance	0.2	-
$\eta_{\text{Na, CNT-CD}}$	Fractional rate of CNT/CD Na <sup>+</sup> reabsorption	0.827*	-
$\eta_{\text{Na, DCT}}$	Fractional rate of DCT Na <sup>+</sup> reabsorption	0.5	-
$\eta_{\text{Na, ALH}}$	Fractional rate of PT Na <sup>+</sup> reabsorption through PT NHE3	0.8	-
$\eta_{\text{Na, reabs-PT,NHE3}}$	Fractional rate of PT Na <sup>+</sup> reabsorption through PT NHE3	0.3	-
$\eta_{\text{Na, reabs-PT,other}}$	Fractional rate of PT Na <sup>+</sup> reabsorption through non-NHE3, non-SGLT2 mechanisms	0.35	-
$\Phi_{\text{Na,ALH0}}$	Rate of sodium delivered to the ALH under baseline conditions	2.02*	$\mu\text{l/min}$
$\Phi_{\text{Na,intake}}$	Sodium intake rate	100	mEq/day
$\tau_{\text{x,SGLT}}$	Time constant for SGLT expression adaptation		
B	LoH flow dependence coefficient	0.75	-
$C_{\text{glu}}$	Plasma glucose concentration	5	mmol/L
$C_{\text{albumin}}$	Plasma albumin concentration	35	mg/dl
$C_{\text{prot}}$	Plasma protein concentration	7	g/dl
$d_{\text{aa0}}$	Nominal afferent arteriole diameter	11	$\mu\text{m}$
$d_{\text{ea0}}$	Nominal efferent arterial diameter	16.5	$\mu\text{m}$
$D_{\text{c,cnt-cd}}$	Connecting tubule/collecting duct effective diameter at control pressure	22	$\mu\text{m}$
$D_{\text{c,dct}}$	Distal convoluted tubule diameter at control pressure	17	$\mu\text{m}$
$D_{\text{c,lh}}$	Loop of Henle diameter at control pressure	17	$\mu\text{m}$
$D_{\text{c,pt}}$	Proximal tubule diameter at control pressure	27	$\mu\text{m}$
$J_{\text{glu,s12}}$	Rate of glucose reabsorption through SGLT2 in the PT S1 and S2 segment per unit length	0.2	mmol/min/mm

$J_{glu,s3}$	Rate of glucose reabsorption through SGLT1 in the PT S3 segment per unit length	0.025	mmol/min/mm
$K_{albumin0}$	Albumin sieving coefficient	0.06	%
$K_{f0}$	Glomerular ultrafiltration coefficient	4	L/min-mmHg
$L_{aa}$	Average afferent arteriole length	73.6*	$\mu m$
$L_{ea}$	Average efferent arteriole length	73.6*	$\mu m$
$L_{CNT-CD}$	Connecting tubule/collecting duct effective length	10	mm
$L_{dct}$	Distal convoluted tubule length	5	mm
$L_{LoH,Asc}$	Ascending loop of Henle length	10	mm
$L_{LoH,Desc}$	Descending loop of Henle length	10	mm
$L_{pt,s1}$	Length of the PT S1 segment	5	mm
$L_{pt,s2}$	Length of the PT S2 segment	5	mm
$L_{pt,s3}$	Length of the PT S3 segment	4	mm
$N_{nephrons}$	Number of nephrons	2e6	-
$[Na]_{ref}$	Normal blood/IF equilibrium sodium concentration	140	mmol/L
$Na_{stored}$	Maximum peripherally stored sodium	2000	Mmol
$P_{c,cnt-cd}$	CNT/CD control pressure	5	mmHg
$P_{c,dt}$	DCT control pressure	6	mmHg
$P_{c,lh,asc}$	Ascending loop of Henle control pressure	7	mmHg
$P_{c,lh,desc}$	Descending loop of Henle control pressure	8	mmHg
$P_{c,pt,s1}$	PT S1 segment control pressure	20.2	mmHg
$P_{c,pt,s2}$	PT S2 control pressure	15	mmHg
$P_{c,pt,s3}$	PT S3 control pressure	11	mmHg

$Q_{\text{water}}$	Rate constant for water transfer between blood and IF	1	1/min
$Q_{\text{Na}}$	Rate constant for sodium transfer between blood and IF	1	1/min
$Q_{\text{Na,storage}}$	Rate constant for sodium storage/release from the peripheral compartment	0.02	1/min
$R_{\text{preaff},0}$	Nominal preafferent arteriole resistance	14	mmHg-min/L
$RC_{\text{albumin}}$	PT capacity for albumin reabsorption	1.7	pg/min/tubule
$\mu$	Blood viscosity	5e-7	mmHg-min
$\text{Water}_{\text{in}}$	Water intake rate	2.1	L/day
$X_{\text{sgl},\text{max}}$	Maximum increase in SGLT expression	30	%

\*Value calculated based on other parameters under baseline conditions

**Table S2. Regulatory mechanisms model parameters**

Parameter	Definition	Value	Units
$\Phi_{\text{Na,md},0}$	Setpoint for sodium flow delivered to the macula densa	0.885*	$\mu\text{l}/\text{min}$
$A_{\text{md-renin}}$	Scaling factor for macula densa renin secretion	0.9	-
$\text{Aldo}$	Aldosterone concentration setpoint	85	pg/ml
$\text{AT1-bound-AngII}_0$	AT1-bound AngII setpoint	16.6*	pg/ml
$C_{\text{Na,MD},0}$	Macula Densa sodium concentration setpoint	63.3*	mEq/L
$G_{\text{CO-tp}}r$	Proportional gain for cardiac output – TPR controller	0.1	-
$G_{\text{Na-vp}}$	Proportional gain for vasopressin control of sodium concentration	0.1	-
$K_{\text{i-tp}}r$	Integral gain for vasopressin control of sodium concentration	0.1	-

$K_{i-vp}$	Integral gain for vasopressin control of sodium concentration	0.005	-
$m_{aldo,cnt-cd}$	Slope factor for aldosterone effect on CNT/CD sodium reabsorption	0.5	-
$m_{aldo,dct}$	Slope factor for aldosterone effect on CNT/CD sodium reabsorption	0.5	-
$m_{AT1-aff}$	Slope factor for AT1-bound AngII effect on afferent resistance	16	-
$m_{AT1-eff}$	Slope factor for AT1-bound AngII effect on efferent resistance	16	-
$m_{AT1-preaff}$	Slope factor for AT1-bound AngII effect on preafferent resistance	16	-
$m_{AT1-pt}$	Slope factor for AT1-bound AngII effect on proximal tubule Na <sup>+</sup> reabsorption	16	-
$m_{autoreg}$	Myogenic autoregulation slope factor	2	-
$m_{TGF}$	Tubuloglomerular feedback signal slope factor	6	-
$P_{preafferent,0}$	Preafferent arteriole pressure setpoint	71*	mmHg
$RIHP_0$	Renal interstitial hydrostatic pressure setpoint	9.66*	mmHg
$S_{aldo-cnt-cd}$	Scaling factor for aldosterone effect on CNT/CD sodium reabsorption	0.2	-
$S_{aldo-dct}$	Scaling factor for aldosterone effect on DCT sodium reabsorption	0.05	-
$S_{AT1-aldo}$	Scaling factor for AT1-bound AngII effect on aldosterone secretion	0.02	-
$S_{AT1-aff}$	Scaling factor for AT1-bound AngII effect on afferent resistance	0.8	-
$S_{AT1-eff}$	Scaling factor for AT1-bound AngII effect on efferent resistance	0.8	-

$S_{AT1-preaff}$	Scaling factor for AT1-bound AngII effect on preafferent resistance	0.8	-
$S_{AT1-pt}$	Scaling factor for AT1-bound AngII effect on proximal tubule Na <sup>+</sup> reabsorption	0.1	-
$S_{autoreg}$	Preafferent autoregulation signal scaling factor	1	-
$S_{TGF}$	Tubuloglomerular feedback signal scaling factor	0.7	-
$S_{P-N,CNT-DC}$	CNT-DC pressure-natriuresis signal scaling factor	0.5	-
$S_{P-N,DCT}$	DCT pressure-natriuresis signal scaling factor	0.1	-
$S_{P-N,LoH}$	LoH pressure-natriuresis signal scaling factor	0.1	-
$S_{P-N,PT}$	PT pressure-natriuresis signal scaling factor	0.5	-

**Table S3. Renin Angiotensin Aldosterone System model parameters**

Parameter	Definition	Value	Units
ACE	ACE activity	47.65*	/min
Chymase	Chymase activity	2.5*	/min
$K_{AT1}$	AT1-receptor binding rate	12.1*	/min
$K_{AT2}$	AT2-receptor binding rate	4*	/min
$K_{d,AngI}$	AngI degradation rate	0.0924	/min
$K_{d,AngII}$	AngII degradation rate	0.146	/min
$K_{d,AT1}$	AT1-bound AngII degradation rate	3.47	/min
$K_{d,renin}$	Renin degradation rate	4	/min

**Table S4. Renal Disease Model Parameters**

Parameter	Definition	Value	Units	Eq.
$\Delta SA_{\max}$	Maximal glomerular surface area increase	50	%	30
$\Delta \text{Perm}$	Decrease in glomerular membrane permeability	0	%	31
$\gamma$	Hill coefficient for glomerular pressure effect on podocyte injury	2	-	32
$\mu_{\text{other,seiv}}$	Podocyte damage due to non-hemodynamic factors	0	-	33
$\tau_{SA}$	Time constant for glomerular hypertrophy			30
$E_{\max}$	Maximum fold increase in sieving coefficient due to glomerular pressure	4	-	32
$K_{m,gp,seiv}$	Glomerular pressure difference that elicits half the maximal effect on albumin sieving	25	mmHg	32
$P_{GC0}$	Glomerular hydrostatic pressure above which podocyte injury occurs	65	mmHg	29
$X_{\text{splt,max}}$	Maximum increase in SGLT expression	30	%	26

**Table S5. Model Initial Conditions**

Variable	Definition	Value	Units
AngI	Angiotensin I	8.164*	pg/mg
AngII	Angiotensin II	5.17*	pg/mg
AT1-bound AngII	AT1-bound AngII	16.6*	pg/mg
AT2-bound AngII	AT2-bound AngII	5.5*	pg/mg
CO	Cardiac Output	5	L/min
BV	Blood Volume	5	L
IFV	Interstitial Fluid Volume	12	L
$Na_{\text{blood}}$	Blood sodium amount	700	mEq
$Na_{\text{IF}}$	Interstitial sodium amount	1400	mEq
$Na_{\text{stored}}$	Stored sodium amount	0	mEq
PRC	Plasma Renin Concentration	17.84	pg/ml